nagra National Cooperative for the Disposal of Radioactive Waste

TECHNICAL REPORT 92-09

TIME-SPACE CONTINUUM DESCRIPTION OF FLUID-ROCK INTERACTION IN PERMEABLE MEDIA

NOVEMBER 1992

P. C. LICHTNER

Geologisches und Mineralogisch-petrographisches Institut, Universität Bern

Hardstrasse 73, CH-5430 Wettingen/Switzerland, Telephone +41-56-37 11 11

nagra National Cooperative for the Disposal of Radioactive Waste

TECHNICAL REPORT 92-09

TIME-SPACE CONTINUUM DESCRIPTION OF FLUID-ROCK INTERACTION IN PERMEABLE MEDIA

NOVEMBER 1992

P. C. LICHTNER

Geologisches und Mineralogisch-petrographisches Institut, Universität Bern

Hardstrasse 73, CH-5430 Wettingen/Switzerland, Telephone +41-56-37 11 11

This report was prepared as an account of work sponsored by Nagra. The viewpoints presented and conclusions reached are those of the author and do not necessarily represent those of Nagra.

ABSTRACT

MPATH (Multiple Reaction Path Model) was developed for modelling coupled processes in geological and engineered systems. Key applications of MPATH include modelling the effect of cement in a repository on the surrounding host rock or oxidation of pyrite in the host rock during the operational phase of the repository. These applications will be dealt with in separate reports, while the present report discusses the basic principles of MPATH.

The feasibility of solving multicomponent mass transport equations incorporating mineral reactions in a homogeneous porous medium over geologic time spans is considered for the case of pure advection. Solution of the mass transport equations is based on a quasi-stationary state approximation in which the time evolution of the geochemical system and the chemical reactions in the multicomponent system are represented by a sequence of stationary states or reaction paths. The method is implemented in the computer code MPATH which solves mass transport equations in a single spatial dimension taking into account (irreversible) mineral precipitation/dissolution reactions and reversible and irreversible aqueous complexing reactions. An adaptable discretisation enables the positions of reaction zones, with widths which vary over many orders of magnitude and which move with greatly differing velocities, to be tracked over geologic time spans. For the code MPATH, there appears to be virtually no practical limitation to the number of chemical species that can be considered, given the computational capacity of present-day, high-performance workstations. The numerical accuracy of the solution to the mass transport equations can be verified through global mass conservation conditions and, in certain cases, by comparing the asymptotic kinetic solution with the corresponding solution to algebraic equations representing local equilibrium conditions for pure advective transport. In this report, the code MPATH is applied to several examples including migration of redox fronts, weathering of alaskite and the hydrothermal alteration of alaskite in a spatially varying temperature field.

ZUSAMMENFASSUNG

MPATH (Multiple Reaction Path Model) wurde zur Modellierung von gekoppelten Prozessen in geologischen und technischen Systemen entwickelt. Wichtige Anwendungen von MPATH sind die Modellierung des Einflusses von Zement in einem Endlager auf das umliegende Wirtgestein oder die Oxidation von Pyrit in Wirtgestein während der Betriebsphase eines Endlagers. Diese Anwendungen werden in separaten Berichten erscheinen; der vorliegende Bericht behandelt die Grundlagen von MPATH.

Mit MPATH können die Massentransport-Gleichungen für rein advektiven Transport eines Mehrkomponentensystems in einem homogenen porösen Medium über geologische Zeiträume gelöst werden unter Berücksichtigung von Mineralreaktionen. Die Lösung der Massentransport-Gleichungen basiert auf einer quasi-stationären Näherung, bei der die zeitliche Entwicklung des geochemischen Systems sowie die chemischen Reaktionen im Mehrkomponentensystem durch eine Abfolge von stationären Zuständen oder Reaktionspfaden dargestellt wird. Zur numerischen Lösung der Massentransport-Gleichungen wurde das Rechenprogramm MPATH erstellt. Es löst die Massentransport-Gleichungen in einer Raumdimension unter Berücksichtigung von (irreversiblen) Fällungs- und Lösungsreaktionen, sowie reversiblen und irreversiblen Reaktionen in der wässrigen Phase. Mit einer sich anpassenden Diskretisierung können die verschiedenen Reaktionszonen über geologische Zeiträume erfasst werden, obwohl sie sich mit äusserst unterschiedlichen Geschwindigkeiten bewegen und ihre Ausdehnung über viele Grössenordnungen variierien kann. Für den Code MPATH bestehen bei der Rechenkapazität der heute verfügbaren Workstations praktisch keine Beschränkungen für die Anzahl der berücksichtigten chemischen Spezies. Die numerische Genauigkeit einer Lösung der Massentransport-Gleichungen kann oft über die Massenerhaltung verifiziert werden. In anderen Fällen kann die asymptotische, numerische Lösung mit der entsprechenden analytischen Lösung für lokale Gleichgewichtsbedingungen mit advektivem Transport verglichen werden. Im vorliegenden Bericht wird MPATH bei der Ausbreitung von Redoxfronten, der Verwitterung von Alaskit und der hydrothermalen Umwandlung von Alaskit in einem räumlich variierenden Temperaturfeld angewendet.

RESUME

On a mis au point le modèle MPATH (Multiple Reaction Path Model) pour modéliser des processus couplés dans des systèmes géologiques et techniques. D'importantes applications de MPATH consistent à modéliser l'influence qu'exerce le ciment d'un dépôt final sur la roche d'accueil environnante, ou encore l'oxydation de la pyrite dans la roche d'accueil au cours de l'exploitation d'un dépôt final. Ces applications font l'objet de différents rapports. Celui-ci décrit les bases de MPATH.

MPATH permet de résoudre les équations du transport de masse pour le transport par pure advection d'un système à plusieurs composantes, dans un milieux poreux homogène et sur des espaces de temps géologiques, compte tenu des réactions minérales. La solution des équations du transport de masse repose sur une approximation quasi stationnaire, pour laquelle l'évolution temporelle du système géochimique ainsi que les réactions chimiques dans le système à plusieurs composantes sont représentées par une série d'états stationnaires ou de chemins de réaction. Cela, en vue de la solution numérique des équations du transport de masse dans une dimension spatiale, compte tenu des réactions (irréversibles) de précipitation et de solution, ainsi que des réactions réversibles et irréversibles dans la phase aqueuse. Une représentation discrète susceptible d'adaptation permet de détecter les différentes zones de réaction sur des espaces de temps géologiques, bien qu'elles se déplacent à des vitesses extrêmement différentes et que leur extension puisse varier de plusieurs ordres de grandeur. Avec le code MPATH et pour la capacité de calcul des stations de travail aujourd'hui disponibles, il n'y a pratiquement pas de limitation au nombre d'espèces chimiques considérées. La conservation de la masse permet souvent de vérifier la précision numérique d'une solution des équations du transport de masse. Dans d'autres cas, on peut comparer la solution numérique asymptotique à la solution analytique correspondante pour des conditions locales d'équilibre avec transport par advection. Dans ce rapport, MPATH est utilisé pour la propagation de fronts redox, l'altération de l'alaskite et la transformation hydrothermale de l'alaskite dans un champ de températures qui varie dans l'espace.

Contents

ABSTRACT i

ZUSAMMENFASSUNG ii

RESUME iii

LIST OF CONTENTS iv

LIST OF TABLES vi

LIST OF FIGURES vii

LIST OF SYMBOLS x

1 INTRODUCTION 1

2 GOVERNING EQUATIONS 5

2.1 Mass Transport Equations 8

2.2 Moving Boundary Problem 9

2.3 Equivalent Form of the Transport Equations 11

2.4 Initial and Boundary Conditions 12

2.5 Kinetic Rate Expressions 13

3 MULTIPLE REACTION PATH FORMULATION 16

3.1 Closed Systems 16

3.2 Stationary States: Open Systems 18

3.3 Time Integration of Mineral Mass Transfer Equations 22

4 NUMERICAL SOLUTION 25

4.1 The Code MPATH 25

4.2 Newton–Raphson Equations 29

4.3 Numerical Accuracy 29

5 EXAMPLES 32

5.1 Single Component System 32

5.2 Redox Problems 35

5.3 Weathering of Alaskite 46

5.4 Hydrothermal Alteration of Alaskite 49

6 DISCUSSION 53

7 CONCLUSION 54

8 ACKNOWLEDGEMENTS 55

9 REFERENCES 56

APPENDIX A: EXPLICIT EXAMPLE OF TRANSPORT EQUATIONS 1

APPENDIX B: TRANSFORMATION OF PRIMARY SPECIES 1

APPENDIX C: JACOBIAN MATRIX 1

List of Tables

1 Results of a local equilibrium calculation for the oxidation of a pyrite bearing host rock containing uraninite and native selenium for the same initial and boundary conditions used in the kinetic calculation presented in Figs. 4–8. . . . 45

2 Initial volume fractions, kinetic rate constants, enthalpies of activation and surface areas used in the calculations describing weathering and hydrothermal alteration of alaskite. 46

List of Figures

1 Schematic illustration of the multiple reaction path formulation of fluid transport and chemical reaction of minerals in a porous medium. With each time step Δt a new state of alteration of the host rock is obtained which determines a new stationary state. 22

2 Time–distance diagram illustrating integration of the mineral mass transfer equations. 25

3 The solute concentration, solid volume fraction and reaction rate for a single component system plotted as a function of distance for an elapsed time of 2,000 years with the parameters given in the text. 35

4 Volume fractions of uraninite (solid curves), native selenium (dashed curves) and pyrite (dotted curves) plotted as functions of distance for the indicated times in units of thousands of years. The host rock contains initial quantities of pyrite (2%), uraninite (1%) and native selenium (1%) by volume. Abbreviations used in the figure are: pyrite (Py), uraninite (Ur), and selenium (Se). 36

5 The reaction rates of uraninite (solid curves), native selenium (dashed curves) and pyrite (dotted curve) plotted as a function of distance for an elapsed time of 500,000 years for the same conditions as in the previous figure. A positive rate denotes precipitation and a negative rate dissolution. Both selenium and uraninite dissolve at their respective upstream boundaries as they become oxidized, and reprecipitate further downstream. Two peaks occur in the selenium precipitation rate. 37

6 The reaction path of a fluid packet after an elapsed time of 500,000 years plotted on a pe–pH diagram. The point labeled A denotes the beginning of the path and the point B the final equilibrium state. The diagram is calculated based on the following constant activities: $\log a_{SO_4^{2-}} = -4$, $\log a_{UO_2^{2+}} = -5$, $\log a_{Fe^{2+}} = -4$, and $\log a_{SeO_3^{2-}} = -4$. 39

7 The pH, pe and Eh plotted as a function of distance for an elapsed time of 500,000 years for the same conditions as in the previous figure. See text for explanation of the calculated changes in pH across the different reaction fronts and the increase in pe as selenium is oxidized. 39

8 The profiles of selected aqueous species plotted as a function of distance for an elapsed time of 500,000 years for the same conditions as in the previous figure. The positions of the selenium, uraninite and pyrite reaction fronts are marked by sharp changes in the concentrations of the appropriate solute species. 40

9 The oxygen fugacity f_{O_2}, pe and pH plotted as a function of distance for an elapsed time of 500,000 years for the same conditions as in the previous figure. 42

10 The positions of reaction fronts for pyrite (long dashed curve), uraninite (solid curve) and selenium (dashed curve) plotted as a function of time for the same conditions as in the previous figure. The corresponding thin lines refer to the local equilibrium calculation. 43

11 Weathering profiles for the alteration of alaskite assuming a Darcy velocity of 1 m y^{-1} for elapsed times of 10,000, 50,000, 100,000 and 1,000,000 years. The precipitation of quartz and chalcedony are suppressed. Kaolinite forms two distinct reaction zones located at the K-feldspar and albite dissolution fronts. Abbreviations used in the figure are: quartz (Qtz), gibbsite (Gbs), kaolinite (Kln), K-feldspar (Kfs), muscovite (Mus) and albite (Ab). 47

12 The variation of pH within the alaskite weathering profile plotted as a function of distance for elapsed times of 10,000 (short dashed), 50,000 (dotted), 100,000 (long dashed) and 1,000,000 (solid) years. 48

13 Gaussian temperature profile. Temperature varies from 25°C at the inlet and outlet to a maximum of 300°C in the center of the column. 49

14 The volume fractions of albite, K-feldspar and quartz plotted as a function of distance for the indicated times resulting from the hydrothermal alteration of alaskite with the composition given in Table 2. On the up-gradient side K-feldspar is replaced by albite as quartz dissolves, and on the down-gradient side albite is replaced by K-feldspar as quartz precipitates. The white area designates porosity which becomes entirely filled with quartz on the down-gradient side of the heat source. 51

15 Mineral reaction rates plotted as a function of distance for an elapsed time of 200,000 years. Note that the reaction rates for albite and K-feldspar are equal in magnitude but opposite in sign indicating that aluminum and silica are approximately conserved by the replacement of K-feldspar by albite. 52

16 Solute concentrations plotted as a function of distance for an elapsed time of 200,000 years. The jumps in concentration of K^+ and $Al(OH)_4^-$ occur at the K-feldspar and albite replacement fronts, respectively. 52

LIST OF SYMBOLS

A Debye–Hückel parameter.

$\mathcal{A}_i^{rev}$ designation for the ith reversibly reacting aqueous complex.

$\mathcal{A}_l^{kin}$ designation for the lth irreversibly reacting aqueous complex.

$\mathcal{A}_j$ designation for the jth primary species.

$\mathbf{A}_m$ affinity of the mth mineral.

$\mathbf{A}_m^{th}$ threshold affinity for the onset of precipitation of the mth mineral.

a_i fit parameters for $\log K$ as function of temperature.

$\mathring{\mathbf{a}}_i$ Debye–Hückel radius parameter for the ith aqueous species.

B Debye–Hückel parameter.

$\dot{b}$ extended Debye–Hückel parameter.

C_{eq} equilibrium concentration.

C_i^{rev} concentration of the ith reversibly reacting aqueous complex.

C_j concentration of the jth primary species.

C_l concentration of the lth irreversibly reacting aqueous complex.

C_l^0 inlet concentration of the lth irreversibly reacting aqueous complex.

C_l^∞ initial concentration of the lth irreversibly reacting aqueous complex.

D diffusion coefficient.

d_m^0 initial grain size of the mth mineral.

$\mathcal{F}(x,\, t;\, \{k\},\, D,\, u)$ general designation for a field variable representing solute concentration or mineral volume fraction.

I ionic strength.

I_i^{rev} reaction rate of the ith reversibly reacting aqueous complex.

I_l^{kin} reaction rate of the lth irreversibly reacting aqueous complex.

I_m reaction rate of the mth mineral.

$\widehat{I}_m$ intrinsic reaction rate of the mth mineral.

J_i flux of the ith reversibly reacting aqueous complex.

J_j solute flux of the jth primary species.

$\mathcal{J}_l$ flux of the lth irreversibly reacting aqueous complex.

$\mathcal{J}_{nn'}$ Jacobian matrix.

K_m equilibrium constant corresponding to the mth mineral.

K_i equilibrium constant for the ith aqueous complex.

K_Δ distribution coefficient.

k_l reaction rate constant associated with the overall reaction of the lth irreversibly reacting aqueous complex.

$k_l^{(f)}$ forward reaction rate constant associated with the lth irreversibly reacting aqueous complex.

$k_l^{(b)}$ backward reaction rate constant associated with the lth irreversibly reacting aqueous complex.

k_m reaction rate constant associated with the overall reaction of the mth mineral.

$\mathcal{L}$ length of flow path.

$\hat{\mathcal{L}}$ differential operator.

$l(t)$ reaction front position.

l_{2n-1}^m, l_{2n}^m upstream and downstream boundaries corresponding to the nth reaction zone of the mth mineral.

$\mathcal{M}_m$ designation for the mth mineral.

M number of reacting minerals.

m_i^{rev} molality of the ith reversibly reacting aqueous complex.

m_j molality of the jth primary species.

m_l^{kin} molality of the lth irreversibly reacting aqueous complex.

N number of primary species.

N_{kin} number of irreversibly reacting aqueous complexes.

N_{rev} number of reversibly reacting aqueous complexes.

n_m number of moles of the mth mineral in a closed system.

Q_m ion activity product corresponding to the mth mineral.

q inverse length characterizing the distance for the solute concentration to reach equilibrium.

R gas constant.

R_j residual function for the jth primary species.

R_l residual function for the lth irreversibly reacting aqueous complex.

s_m surface area of the mth mineral per unit volume of bulk rock.

$T(x, t)$ temperature field at position x and time t.

t time.

t' travel time of a fluid packet.

u Darcy fluid velocity.

$\bar{V}_m$ molar volume of the mth mineral.

v average fluid velocity.

v_l velocity of the lth reaction front.

x spatial coordinate.

z_i valence of the ith solute species.

α subscript designating a primitive primary species.

$\bar{\alpha}$ subscript designating a non-primitive primary species.

γ_j, γ_i aqueous activity coefficients for the jth primary species and ith complex.

Δx spatial step size.

Δt time step.

$\Delta H_m^{\dagger}$ activation enthalpy corresponding to the mth mineral.

$\zeta_m(x, t)$ reaction index corresponding to the mth mineral.

$\vartheta(x)$ Heaviside function.

λ finite difference parameter.

ν_{ji}^{rev} stoichiometric reaction matrix for reversibly reacting aqueous complexes.

ν_{jl}^{kin} stoichiometric reaction matrix for irreversibly reacting aqueous complexes.

ν_{jm} stoichiometric reaction matrix for mineral reactions.

$(\nu^{-1})_{m\bar{\alpha}}$ inverse matrix to $\nu_{\bar{\alpha}m}$.

$\tilde{\nu}_{\alpha\bar{\alpha}}$ stoichiometric matrix for a conserved quantity.

$\hat{\nu}_{im}$ stoichiometric matrix of the ith activated complex associated with the overall reaction of the mth mineral.

ξ_m reaction progress variable of the mth mineral.

ρ_0 density of pure water.

σ Temkin's average stoichiometric number.

τ_0 time for mineral to completely dissolve at inlet.

ϕ porosity.

ϕ_m volume fraction of the mth mineral.

ϕ_m^{∞} initial volume fraction of the mth mineral.

Ψ_j generalized concentration of the jth primary species.

Ψ_j^0 generalized inlet concentration of the jth primary species.

Ψ_j^{∞} generalized initial concentration of the jth primary species.

Ω_j generalized flux of the jth primary species.

1. INTRODUCTION

A characteristic feature of many geochemical processes involving fluid-rock interaction in natural systems is the long time spans over which these processes typically evolve. Such diverse phenomena as weathering, diagenesis, formation of ore deposits and migration of highly toxic radionuclides from a nuclear waste repository take place extremely slowly over thousands to millions of years or more. Rates of chemical reactions occurring in these systems are often too slow to observe their effects in the laboratory. One of the central problems facing a quantitative description of fluid-rock interaction in natural systems which takes into account both time and space as descriptive variables is solving the governing transport equations over the long time spans associated with natural systems. An equally challenging problem involves the formation of mineral alteration zones consisting of different mineral assemblages which propagate with time. The mathematical description of this problem is referred to as a moving boundary problem. Mineral alteration zones migrate in response to transport by advection, dispersion and diffusion with widths ranging from millimeters to hundreds of meters or more within a given system. Reaction fronts associated with the boundaries of mineral alteration zones may be sharp, approaching delta function singularities in the case of transport controlled reaction rates in the limiting case of local chemical equilibrium, or smooth functions of distance for slower surface controlled kinetic reaction rates. Redox reactions are typically associated with extremely sharp reaction fronts, limited only by the grain size of the porous medium. As a consequence of the large variation in length scales possible, and the extremely long geologic time spans involved, the moving boundary nature of the transport–reaction problem presents special difficulties for solving numerically the governing transport equations. These problems are further compounded in multicomponent systems which involve large numbers of chemically reacting species.

The purpose of this contribution is to demonstrate the feasibility of integrating multicomponent mass transport equations over time spans appropriate to natural systems, taking into account both kinetics of mineral reactions and the moving boundary aspects of the problem. The proposed method is applied to pure advective transport in a homogeneous porous medium involving a single spatial dimension assuming constant porosity and permeability. However, the same technique is also applicable to transport by diffusion and dispersion and to more than one spatial dimension. Variations in porosity and permeability resulting from chemical reaction

can also be taken into account provided the necessary constitutive relations are known. The approach presented here represents an extension of the techniques developed by Lichtner [1988] based on the quasi-stationary state approximation. In this approximation the time evolution of a geochemical system is represented by a sequence of stationary states or reaction paths. The quasi-stationary state approximation is rigorously based on the exact, time-dependent formulation of the mass transport equations.

The method described here is implemented in the computer code **MPATH** (**M***ultiple Reaction* **PATH** *Model*). The code **MPATH** calculates a sequence of reaction paths for a specified set of minerals reacting with an inlet fluid of specified composition. Helgeson [1968] developed a single reaction path formulation to describe the alteration of minerals in a geochemical system for both open and closed systems. This approach was based originally on reaction progress as the descriptive variable. Later time was incorporated explicitly into the description through reaction kinetics [Helgeson and Murphy, 1983]. This technique has found extensive application to understanding the behavior of complex geochemical systems. However, including time and space coordinates within this framework is not possible in the presence of moving boundaries such as characterize the transport-reaction problem. Nevertheless a time-space description can be closely related to Helgeson's original single reaction path approach. By considering many reaction paths, with each path dependent on the preceding path through alteration of minerals contained in the host rock, it is possible to describe the evolution of a geochemical system in both time and space. Such an approach is referred to as a multiple reaction path formulation [Lichtner, 1986; Lichtner, 1988]. This approach has been successfully applied to a description of weathering and transport of uranium at the Osamu Utsumi uranium mine at Poços de Caldas, Brazil, resulting in qualitative agreement with field observations [Lichtner and Waber, 1992]. In addition the method has been applied to supergene enrichment of a porphyry copper deposit [Lichtner and Biino, 1992; Biino and Lichtner, 1992].

The quasi-stationary state approximation is fundamentally different from a finite difference or finite element approach to solving the transient mass transport equations (see e.g. Steefel and Van Cappellen [1990]). These latter formulations provide, in principle, an exact solution to the governing mass conservation equations. However, provided the quasi-stationary state approximation is sufficiently accurate, it must yield the same results as these more precise

methods. The finite-difference approach may be understood intuitively by considering a row of boxes containing both fluid and rock. Each box represents a node point making up the finite-difference grid. A time step is represented by pouring the fluid contained in one box into its neighboring box. After this operation is completed for all the boxes, the fluid in each box is no longer in equilibrium with the minerals in the box. Depending on whether a local equilibrium or kinetic representation of mineral reaction rates is being deployed, the fluid is allowed to react either until equilibrium is achieved, or for a duration of time equal to the transport time step. As a consequence, the fluid composition and mineral abundances in each box are altered due to chemical reaction. Essential to this approach is that changes to both mineral abundances and composition of the aqueous solution are computed simultaneously during each time step. Because of the tight coupling between minerals and fluid, this approach is computationally extremely time consuming. For a significant change in mineral abundances to occur, many steps must be taken as a consequence of the low solubilities of most minerals. Furthermore, in order that the time step is not limited to unreasonably small values by stability considerations a large grid spacing is required, which may reduce significantly the accuracy of the solution.

By contrast, the quasi-stationary state approximation leads to a weak coupling between minerals and the aqueous solution. In this method the fluid composition is calculated independently of changes in mineral abundances. First, the fluid composition and mineral reaction rates are determined at each point along the flow path before the alteration of minerals is allowed to take place. The fluid composition is represented by a stationary state formed by the reaction of a single packet of fluid with the minerals it encounters along the flow path. From the mineral reaction rates, the changes in mineral abundances can then be calculated over a time step that is large compared to the time to transport fluid from one box to the next associated with the finite-difference approach. Because a much longer time step, limited only by the time during which the fluid composition remains stationary, can be afforded compared to the time step associated with finite-difference or finite-element algorithms, this approach allows calculations of complex, multicomponent systems to be carried out over geologic time spans. Any particular stationary state has a finite lifetime. As minerals continue to react and their surface areas and zone boundary positions change with time, eventually the current stationary state no longer represents a reasonable approximation and a new stationary state must be computed corresponding to the altered host rock.

The validity of the quasi-stationary state approximation is based on a physical property encountered in most systems involving fluid-rock interaction, that any particular species is generally much more concentrated in solid phases compared to its concentration in an aqueous solution (Ortoleva et al., 1987; Lichtner, 1988). As a consequence the concentrations of solute species rapidly become stationary in time compared to the time scale during which minerals can be significantly altered, and thus, for all practical purposes, the fluid composition forms a stationary state. This approximation would be expected to breakdown for very concentrated brines or melts. In addition, the time variation of other quantities, such as temperature and the composition of the inlet fluid, must be slow compared to the time to establish a stationary state. Thus, for example, it would not be feasible to incorporate seasonal variations in solute concentrations within the quasi-stationary state approximation and an average value must be assumed instead. The main advantage of this approximation, compared to a finite-difference approach applied to the transient mass conservation equations, is the possibility of carrying out time-space calculations of complex, natural geochemical systems over geologic time spans. Further, the method takes into full account moving boundaries associated with mineral alteration zones.

After developing the general theory, several examples are presented which illustrate the multiple reaction path approach using the computer code **MPATH**. This code solves a coupled system of ordinary differential equations describing pure advective mass transport and chemical reaction in a homogeneous porous medium assuming constant porosity and permeability. Chemical reactions provided in **MPATH** consist of reversible and irreversible homogeneous reactions within the aqueous phase including ion pairing, complexing and redox reactions; and irreversible heterogeneous reactions of minerals. The rates of irreversible mineral reactions are described by kinetic rate laws based on transition state theory of which several different forms are available. An adaptive grid allows the position of reaction zones of essentially arbitrary width to be tracked simultaneously over geologic time spans. There appears to be virtually no practical limitation to the number of chemical species that can be included in the code without rendering the computational effort beyond the bounds of a high-performance workstation.

In addition to this report a programmers handbook and users guide will be made available in the near future. A thorough description of the theoretical basis of the code can be found in

Lichtner (1988).

2. GOVERNING EQUATIONS

Mass transport equations representing a time–space description of advective and diffusive/dispersive transport of solute species combined with chemical reactions are formulated using the continuum theory of mixtures (Lichtner, 1985). In this approach mass conservation relations are established for a representative elemental volume (REV) of the system. A REV is chosen to be smaller than the characteristic length scale of the phenomena being investigated, but large enough to include many mineral grains. Within a REV the properties of the system such as solute concentration, mineral modal abundance, porosity and permeability are presumed constant. A well-mixed, closed system in which transport can be disregarded, is represented by a single REV.

Chemical reactions included in the description may be conveniently divided into homogeneous reactions taking place within the aqueous phase and heterogeneous reactions taking place between minerals and aqueous species. Homogeneous reactions consist of ion pairing, complexing and redox reactions. In order to provide for decoupling of aqueous redox pairs, essential for a description of many geochemical systems especially at low temperatures, both kinetic and local equilibrium representations of rates of homogeneous reactions are included in the description. In the development which follows, kinetic rate laws are used to describe the reaction of minerals with the aqueous solution. There are significant advantages to using a kinetic description of mineral reaction rates compared to a local chemical equilibrium description. First of all, a kinetic description is more fundamental than one based on local equilibrium. Local equilibrium is the mathematical limiting case of a kinetic description in which the reaction rate constant tends towards infinity. Therefore it is always possible to obtain the local equilibrium description from the kinetic formulation merely by choosing the product of the kinetic rate constant and mineral surface area sufficiently large. Another reason for employing a kinetic formulation is that it provides, as part of the solution to the differential equations, the correct reaction zone sequence. In a local equilibrium description based on the quasi-stationary state approximation the reaction zone sequence can only be determined by trial and error (Lichtner, 1991).

Ion-exchange reactions are not considered in the development which follows. It is assumed that for the very long time spans that are the main interest of this work, ion-exchange reactions play only a minor role in determining the major element chemistry. This, however, may not always be the case and, if necessary, such reactions can be easily included. However, the propagation of ion-exchange reaction fronts is a strictly transient behavior, which is not possible to describe within the quasi-stationary state approximation [Schechter et al., 1987].

For a system in equilibrium it makes no difference in what form the chemical reactions are written, the only requirement is that all reactions are independent of one another. However, for irreversible reactions the rate mechanism is dependent on the particular form of the reaction. Chemical reactions are not necessarily elementary, but usually involve several elementary steps which may occur in parallel or series. Usually kinetic rate laws for minerals, such as hydrolysis reactions, are formulated as overall reactions. To describe the chemical reactions occurring in a geochemical system it is convenient to introduce a minimal set of primary species denoted by $\{\mathcal{A}_j\}$, $(j = 1, \cdots, N)$, in terms of which all other species can be derived by chemical reactions. Aqueous complexes are denoted by $\mathcal{A}_i^{rev}$ $(i = 1, \cdots, N_{rev})$, and $\mathcal{A}_l^{kin}$ $(l = 1, \cdots, N_{kin})$, corresponding to reversibly and irreversibly reacting species, respectively. Minerals are denoted by $\mathcal{M}_m$ $(m = 1, \cdots, M)$. Homogeneous reactions are of two types depending on whether the reactions are reversible or irreversible. They are assumed to have similar forms given by:

$$\sum_{j=1}^{N} \nu_{ji}^{rev} \mathcal{A}_j \rightleftharpoons \mathcal{A}_i^{rev}, \tag{1}$$

for reversible reactions, and

$$\sum_{j=1}^{N} \nu_{jl}^{kin} \mathcal{A}_j \rightleftharpoons \mathcal{A}_l^{kin}, \tag{2}$$

for irreversible reactions. Irreversible heterogeneous reactions have the form

$$\sum_{j=1}^{N} \nu_{jm} \mathcal{A}_j \rightleftharpoons \mathcal{M}_m. \tag{3}$$

The matrices ν_{ji}^{rev}, ν_{jl}^{kin} and ν_{jm} denote the respective stoichiometric reaction coefficients. The reactions are arranged in such a manner that the stoichiometric coefficients of reversible and irreversible aqueous complexes and minerals are unity. This may always be achieved as demonstrated by Lichtner (1985). The choice of primary species is not unique, and may be chosen from any of the reversibly reacting aqueous species, provided only that they form a

complete set in the sense of Eqns.(1), (2) and (3). Primary species may not be chosen from the set of irreversibly reacting complexes which must remain as independent species. Those species not included among the primary species are referred to as secondary species.

In general, there does not exist a simple expression for the rate of an overall reaction involving more than one mineral, which may be quite complicated involving time and space dependent reaction coefficients and only represents an approximate description of the actual reactions taking place in the system. The reactions as written above do not include more than one product mineral in a single reaction, and thus are expressed as congruent dissolution or precipitation reactions. Actually the form of the reactions as written includes reactions between several minerals as a special case and represents the most general description possible. Incongruent mineral-mineral reactions, which often occur in real systems, result from several "congruent" reactions taking place simultaneously.

As an example, consider the hydrolysis reactions of potassium feldspar and kaolinite. These are expressed individually as the overall reactions:

$$K^+ + Al^{3+} + 3SiO_2 + 2H_2O - 4H^+ \rightleftharpoons KAlSi_3O_8, \tag{4}$$

and

$$2Al^{3+} + 2SiO_2 + 5H_2O - 6H^+ \rightleftharpoons Al_2Si_2O_5(OH)_4. \tag{5}$$

A common reaction in weathering of feldspar is the formation of clay minerals such as kaolinite. To write a single overall reaction describing the dissolution of K-feldspar and precipitation of kaolinite would require making some additional assumptions beyond what is already assumed in writing the above two *independent* hydrolysis reactions. For example, an assumption often made in this case is conservation of aluminum leading to the overall reaction:

$$2KAlSi_3O_8 + 2H^+ + H_2O \rightarrow Al_2Si_2O_5(OH)_4 + 2K^+ + 4SiO_2. \tag{6}$$

However this is only an approximation, and in some cases a very bad approximation—for example in the presence of organic acids. A more precise procedure, which does not reduce the number of degrees of freedom, is to keep the above two reactions independent, and let the transport equations themselves decide whether under the particular circumstances aluminum is conserved or not.

2.1. Mass Transport Equations

Transport equations representing conservation of mass are derived by balancing the flux of solute species entering and leaving a REV with the change in solute concentration within the REV and the contribution from homogeneous and heterogeneous chemical reactions taking place between the solute species and minerals contained in the REV. For the general case of transport by advection, diffusion and dispersion, mass transport equations for aqueous species incorporating simultaneous chemical reactions as described by the reactions given in Eqns.(1), (2) and (3) in a time-space continuum description take the form (Lichtner, 1985):

$$\frac{\partial}{\partial t}\left(\phi C_j\right) + \frac{\partial J_j}{\partial x} = -\sum_{m=1}^{M} \nu_{jm} I_m - \sum_{i=1}^{N_{rev}} \nu_{ji}^{rev} I_i^{rev} - \sum_{l=1}^{N_{kin}} \nu_{jl}^{kin} I_l^{kin}, \tag{7}$$

for the jth primary species with concentration C_j,

$$\frac{\partial}{\partial t}\left(\phi C_i^{rev}\right) + \frac{\partial J_i^{rev}}{\partial x} = I_i^{rev}, \tag{8}$$

for the ith reversibly reacting aqueous complex with concentration C_i^{rev}, and

$$\frac{\partial}{\partial t}\left(\phi \mathcal{C}_l\right) + \frac{\partial \mathcal{J}_l}{\partial x} = I_l^{kin}, \tag{9}$$

for the lth irreversible aqueous complex with concentration $\mathcal{C}_l$. In what follows the subscripts j and m are reserved for primary species and minerals, respectively. The volume fraction ϕ_m of the mth mineral satisfies the mass transfer equation

$$\frac{\partial \phi_m}{\partial t} = \bar{V}_m I_m, \tag{10}$$

in which a flux term is absent. In these equations J_j denotes the flux of the jth primary species consisting of contributions from advection and diffusion given by

$$J_j = -\phi D \frac{\partial C_j}{\partial x} + u C_j, \tag{11}$$

with similar expressions for reversibly and irreversibly reacting complexes with corresponding fluxes denoted by J_i^{rev} and $\mathcal{J}_l$, where ϕ denotes the porosity, D the diffusion coefficient and u the Darcy fluid velocity. The quantities I_i^{rev} and I_l^{kin} denote, respectively, the reaction rates for formation of the ith reversibly and lth irreversibly reacting complex. The rate of the mth mineral with molar volume $\bar{V}_m$ is denoted by I_m.

The porosity and mineral volume fractions may be related by the equation

$$\phi = 1 - \sum_{m=1}^{M} \phi_m. \tag{12}$$

Note that the porosity defined by this expression refers to the *total* porosity which need not be identical to the *flow* porosity which enters into the transport equations. In what follows, the effects on the flow rate due to changes in porosity and permeability resulting from chemical reactions are neglected. However, these effects could be potentially very important in self-sealing systems, or in systems where large changes in porosity (and permeability) occur. The above relation between total porosity and mineral volume fractions can provide a useful estimate of the change in flow porosity resulting from reactions with minerals. By monitoring the change in porosity as determined from Eqn.(12), it is possible to ascertain the validity of the assumption of constant porosity.

The concentrations of reversibly reacting solute species are obtained from the mass action equations

$$C_i^{rev} = K_i \gamma_i^{-1} \prod_{j=1}^{N} (\gamma_j C_j)^{\nu_{ji}}, \tag{13}$$

which express their concentrations in terms of the concentrations of primary species. In this expression K_i denotes the equilibrium constant, and γ_j, γ_i denote activity coefficients of the subscripted species. The mass action equations eliminate the need for Eqn.(8) describing the transport of reversibly reacting complexes, thereby reducing the total number of solute transport equations necessary to solve to Eqns.(7) and (9). The reaction rate for the ith reversibly reacting aqueous complex can be calculated from Eqn.(8), once the transport equations have been solved.

2.2. Moving Boundary Problem

Each reaction zone is delimited by the pair of zone boundaries $(l^m_{2n-1},\, l^m_{2n})$, giving the positions of the end points of the nth zone corresponding to the mth mineral, with $n = 1,\, 2,\, \cdots$. These quantities may be conveniently defined in terms of the mineral volume fractions $\phi_m(x,\, t)$ which provide the spatial distribution of minerals along the flow path at any instant in time. The region of space over which ϕ_m is non-zero is represented by the zone boundary positions $l^m_n(t)$, defined such that

$$\phi_m(x,\, t) > 0 \quad \text{for} \quad l^m_{2n-1}(t) < x < l^m_{2n}(t), \quad (n = 1,\, 2,\, \cdots). \tag{14}$$

A given mineral may occur in more than one reaction zone. The zone boundary velocity is obtained by differentiating the zone boundary position with respect to time.

The moving boundary aspect of the transport–reaction problem is taken into account through the reaction index $\zeta_m(x,\, t)$ corresponding to the mth mineral, which has the values unity or zero. The reaction index serves as a flag to indicate the possibility for reaction to take place, depending on whether the mineral is actually present or not, at a particular point along the flow path. This quantity is included as a multiplicative factor in the definition of the mineral reaction rate according to the relation

$$I_m(x,\, t) \;=\; \zeta_m(x,\, t)\, \widehat{I}_m(x,\, t), \tag{15}$$

where $\widehat{I}_m$ refers to the intrinsic mineral reaction rate. It has the value one if the mth mineral is present or begins to precipitate if not present, and zero if the mth mineral is under-saturated but is not present. For the case in which the mineral is in equilibrium with the fluid, the reaction rate itself vanishes, and the value of the factor ζ_m can be either zero or unity. Expressions for the intrinsic rate are defined below. The reaction index $\zeta_m(x,\, t)$ is defined explicitly by the relations

$$\zeta_m(x,\, t) \;=\; \begin{cases} 1 & \text{if} \quad \left[\phi_m(x,\, t) > 0\right] \text{ or } \left[\phi_m(x,\, t) = 0 \text{ and } \mathbf{A}_m(x,\, t) \le \mathbf{A}_m^{th} \le 0\right] \\ 0 & \text{if} \quad \phi_m(x,\, t) = 0 \text{ and } \mathbf{A}_m(x,\, t) > 0 \end{cases}, \tag{16}$$

where the quantity $\mathbf{A}_m$ refers to the affinity of the overall precipitation/dissolution reaction of the mth mineral, defined according to the expression

$$\mathbf{A}_m \;=\; -RT \ln\left[K_m Q_m\right], \tag{17}$$

where K_m denotes the equilibrium constant for the reaction as written in Eqn.(3), and Q_m designates the ion activity product defined by

$$Q_m \;=\; \prod_{j=1}^{N} \left(\gamma_j C_j\right)^{\nu_{jm}}. \tag{18}$$

According to its definition, the affinity is positive for dissolution or under-saturation, and negative for precipitation or super-saturation. The quantity $\mathbf{A}_m^{th}$ denotes the threshold affinity setting the onset of nucleation, providing for super-saturation of kinetically inhibited minerals. Equilibrium occurs when the affinity vanishes or, equivalently,

$$K_m Q_m \;=\; 1. \tag{19}$$

2.3. Equivalent Form of the Transport Equations

The transport equations for the primary species can be cast in an alternative form by eliminating the reaction rates I_i^{rev} and I_i^{kin} corresponding to reversible and irreversible aqueous complexes, respectively, from the transport equations for the primary species, Eqn.(7). Solving Eqns.(9) and (8) for I_i^{kin} and I_i^{rev} and substituting the result into Eqn.(7) yields the equation

$$\frac{\partial}{\partial t}(\phi\Psi_j) + \frac{\partial\Omega_j}{\partial x} = -\sum_{m=1}^{M}\nu_{jm}I_m, \tag{20}$$

where the quantities Ψ_j and Ω_j, referred to respectively as the generalized concentration and flux (Lichtner, 1985), are defined by

$$\Psi_j = C_j + \sum_{i=1}^{N_{rev}}\nu_{ji}^{rev}C_i^{rev} + \sum_{l=1}^{N_{kin}}\nu_{jl}^{kin}\mathcal{C}_l, \tag{21}$$

and

$$\Omega_j = J_j + \sum_{i=1}^{N_{rev}}\nu_{ji}^{rev}J_i^{rev} + \sum_{l=1}^{N_{kin}}\nu_{jl}^{kin}\mathcal{J}_l. \tag{22}$$

Note that in general Ψ_j may take on positive or negative values (Lichtner, 1985). For the case where the reaction coefficients are all positive, Ψ_j represents the total concentration of the respective species. This is demonstrated in Appendix A where the transport equations are written out in full for an example involving the alteration of K-feldspar. For the special case where the diffusion coefficient is independent of the species, as assumed here, Eqn.(20) simplifies to an equation involving only the quantity Ψ_j according to the expression

$$\left[\frac{\partial}{\partial t}\phi - \phi D\frac{\partial^2}{\partial x^2} + u\frac{\partial}{\partial x}\right]\Psi_j = -\sum_{m=1}^{M}\nu_{jm}I_m. \tag{23}$$

For species-dependent diffusion coefficients, however, it is necessary to use the individual species concentrations to ensure charge balance (Lichtner, 1985).

The alternative form of the primary species transport equations involves only the reaction rates of minerals. Equation (20) together with Eqns.(9) and (10) and the mass action equations, Eqn.(13), provide an equivalent description of the system. The incorporation of reversibly reacting aqueous complexes results in a significant simplification of the problem. Nevertheless, due to the kinetic rate terms of the right hand side of Eqns.(20), (9) and (10), these equations represent a formidable set of stiff, non-linear partial differential equations. To be of any use for describing natural geochemical processes evolving over geologic time spans, it must be possible

to integrate these equations over time spans of hundreds of thousands to millions of years or more for multicomponent systems. Typically these equations might involve up to 15 primary species, 100 aqueous complexes and as many minerals.

2.4. Initial and Boundary Conditions

To solve the transport equations it is necessary to impose appropriate initial and boundary conditions. Initial conditions specify the state of the system at $t = 0$, providing values of the modal composition of the unaltered host rock and the composition of the fluid initially in contact with the minerals in the rock. The initial rock composition need not be uniform, but could represent an initially zoned rock, for example. The initial fluid composition may include the presence of a water table. Boundary conditions specify the composition or flux of the infiltrating fluid at the inlet and outlet of the column. For many geochemical systems these quantities are difficult to obtain. It may not be possible to easily identify a starting time "$t = 0$", as natural systems often involve several different continuously overlapping processes. Modal abundance data of minerals has been largely ignored by field geologists and much of this data for altered rock has been lost due to the sampling procedures used and to mining operations. However, mineral modal abundances provide, perhaps, our only record of the past history of many geochemical systems during their evolution in time and space. The boundary fluid composition is well-known for weathering environments, but only for present day conditions. However, the presence of a soil zone may strongly affect the pH and CO_2 content of the inlet fluid.

Provided the initial fluid composition is in equilibrium with the host rock, it is not necessary to include it in a description involving pure advective transport, since the initial fluid is flushed out of the column. In symbols the initial conditions are given by

$$\Psi_j(x, 0) = \Psi_j^{\infty}(x), \tag{24}$$

$$C_l(x, 0) = C_l^{\infty}(x), \tag{25}$$

and

$$\phi_m(x, 0) = \phi_m^{\infty}(x), \tag{26}$$

where Ψ_j^∞ and C_l^∞ represent the concentration of the jth primary species and lth irreversibly reacting species in the fluid initially in contact with the host rock, and ϕ_m^∞ represents the initial modal composition of the mth mineral in the unaltered rock. The boundary conditions at the inlet are given by

$$\Psi_j(0,\, t) \;=\; \Psi_j^0(t), \tag{27}$$

and

$$C_l(0,\, t) \;=\; C_l^0(t), \tag{28}$$

referred to as concentration boundary conditions, where Ψ_j^0 and C_l^0 represent the composition of jth primary species and lth irreversibly reacting species in the inlet fluid, respectively. As indicated, these quantities may vary with time or distance. In addition, in a transient description, it is necessary to specify boundary conditions at the outlet. These conditions are not needed in what follows, because focus is on obtaining stationary state solutions to the transport equations (see Lichtner (1985)).

2.5. Kinetic Rate Expressions

For irreversible reaction of minerals and aqueous complexes, constitutive relations must be supplied which express the reaction rate as a function of solution composition, reacting surface area in the case of minerals, and the local temperature and pressure of the system. One form for the reaction rate I_l^{kin} for irreversibly reacting aqueous complexes, corresponding to Eqn.(2), is as an elementary reaction:

$$I_l^{kin} \;=\; k_i^{(f)} \prod_{\nu_{jl}^{kin}>0} (\gamma_j m_j)^{\nu_{jl}^{kin}} - k_l^{(b)}\, \gamma_i m_l^{kin} \prod_{\nu_{jl}^{kin}<0} (\gamma_j m_j)^{-\nu_{jl}^{kin}}, \tag{29}$$

where $k_l^{(f)}$ and $k_l^{(b)}$ denote the forward and backward rate constants respectively and m_l^{kin} denotes the molality of the lth irreversibly reacting complex. As defined the rate is positive for association and negative for dissociation of the complex. An alternative form expresses the rate as an overall reaction according to the expression

$$I_l^{kin} \;=\; -k_l \left\{ 1 - \exp(-\mathbf{A}_l^{kin}/RT) \right\}, \tag{30}$$

where $\mathbf{A}_l^{kin}$ denotes the affinity, defined analogously to Eqn.(17), of the overall reaction.

The hydrolysis of silicate minerals may be described by rate laws based on transition state theory (Aagaard and Helgeson, 1982; Helgeson et al., 1984), leading to an expression for the rate of the form

$$\hat{I}_m = -s_m k_m \left(\prod_i a_i^{\hat{\nu}_{im}} \right) \left\{ 1 - \exp(-\mathbf{A}_m / \sigma RT) \right\}, \tag{31}$$

where $\mathbf{A}_m$ denotes the chemical affinity for the mth mineral defined in Eqn.(17), s_m denotes the effective reacting surface area per unit volume of bulk porous medium, k_m denotes the reaction rate constant, $\hat{\nu}_{im}$ designates the stoichiometric matrix for the elementary surface reaction, R denotes the gas constant, and T denotes the temperature. The quantity σ denotes Tempkin's average stoichiometric number which, in the case of a single rate limiting step, represents the ratio of the rate of decomposition of the activated complex to that of the overall reaction (Aagaard and Helgeson, 1982). The reaction rate of the mth mineral is positive for precipitation and negative for dissolution. The rate constant is in general a function of temperature and pressure as well as solution composition. For example, it may depend on the pH and ionic strength. For constant pressure the variation in the rate constant with temperature is given by the expression (Helgeson et al., 1984):

$$k_m(T) = \frac{T k_m^0}{T_0} \exp\left[-\left(\frac{1}{T} - \frac{1}{T_0} \right) \frac{\Delta H_m^\dagger}{R} \right], \tag{32}$$

where k_m^0 denotes the rate constant at some given temperature T_0, usually taken at the standard state condition of 25°C, and $\Delta H_m^\dagger$ denotes the enthalpy of activation.

An essential feature of Eqn.(31) is that it implies that the reaction rate vanishes at equilibrium, as it must. Because of this property, this expression is still useful for minerals for which the kinetic rate constant is only poorly known, or for those cases in which the rate constant represents an effective rate constant which depends on the geometry of the system in the presence of a boundary layer (Murphy et al., 1991; Lichtner, 1991). In such cases the rate expression may be considered as a pseudo-kinetic rate law, enabling departures from equilibrium to be investigated. It is certainly no worse than the assumption of local equilibrium, even though it may be necessary to use a somewhat arbitrary value for the rate constant, since it approaches this limit as the rate constant increases without bound.

Far from equilibrium the reaction rate has two distinct limiting forms corresponding to

precipitation ($\mathbf{A}_m < 0$) and dissolution ($\mathbf{A}_m > 0$) given by

$$\widehat{I}_m = \begin{cases} k_m s_m \left(\prod_i a_i^{\hat{\nu}_{im}}\right) \exp[|\mathbf{A}_m|/\sigma RT] & \text{(precipitation, } |\mathbf{A}_m| \gg RT) \\ \\ -k_m s_m \left(\prod_i a_i^{\hat{\nu}_{im}}\right) & \text{(dissolution, } \mathbf{A}_m \gg RT) \end{cases} \tag{33}$$

Thus far from equilibrium the rate becomes constant for dissolution, whereas for precipitation the rate grows exponentially with the chemical affinity. At some point it is to be expected that the form of the rate expression for precipitation must breakdown as diffusion of solute species to the reacting surface becomes the rate limiting step. Close to equilibrium the rate is proportional to the chemical affinity according to the expression

$$\widehat{I}_m = \frac{k_m s_m}{\sigma RT} \left(\prod_i a_i^{\hat{\nu}_{im}}\right) A_m. \tag{34}$$

This form of the rate law does not provide for different mechanisms for precipitation and dissolution as has been suggested by recent experiments (Nagy et al., 1991).

The mineral surface area appearing in the expression for the mineral reaction rate may be related to the mineral volume fraction by an empirical equation of the form

$$s_m = s_m^0 \left(\frac{\phi_m}{\phi_m^\infty}\right)^{2/3}, \tag{35}$$

where s_m^0 denotes the initial surface area. This constitutive relation for the dependence of the surface area on reaction is highly idealized, however. It leads to the correct behavior as the mineral completely dissolves, but it does not allow for an increase in surface area caused, for example, by the formation of etch pits during dissolution. Fortunately, for the very long time spans of interest here, the specific details of the kinetic rate term has only a weak affect on the asymptotic behavior of the system (Lichtner, 1992). The initial surface area may be estimated from the measured grain size of the unreacted minerals. Assuming cubical grains the initial surface area can be expressed according to the equation

$$s_m^0 = \frac{6}{d_m^0} \phi_m^\infty, \tag{36}$$

where d_m^0 denotes the initial mineral grain size. This equation assumes that the porosity is sufficiently small compared to the mineral volume that it may be neglected.

3. MULTIPLE REACTION PATH FORMULATION

For most systems of geologic interest the mass transport equations must be solved numerically. This represents a formidable problem and approximations must be introduced in order to carry out calculations over geologic time spans in reasonable amounts of computer time. The approach used here is based on the quasi-stationary state approximation, or multiple reaction path formulation (Lichtner, 1986, 1988, 1991). A reaction path in an open or closed system refers to a description of the state of the system as it evolves with increasing reaction progress or time resulting from chemical reactions. For a system involving fluid flow, a reaction path may be parameterized by the travel time of a packet of fluid as it traverses the flow path. Before formulating the problem for open systems, the much simpler case of a closed system is considered first.

3.1. Closed Systems

In a closed system, which is well-mixed so that transport by diffusion may be neglected, the reaction path followed by the system in which an assemblage of minerals reacts with a fluid of specified composition is obtained by solving the following system of ordinary differential equations

$$\frac{d\Psi_j}{dt} = -\sum_{m=1}^{M} \nu_{jm} I_m, \tag{37}$$

and

$$\frac{dn_m}{dt} = I_m, \tag{38}$$

where n_m denotes the amount of the mth mineral precipitated or dissolved in units of moles (kg H_2O)$^{-1}$ with $\Psi_j(t)$ defined in Eqn.(21) and the reaction rate I_m given by Eqn.(31). In this equation concentrations are expressed in molality units and the reaction rate in units of moles (kg H_2O)$^{-1}$ s^{-1}. Change in volume of the system with reaction is neglected. For brevity, reactions involving irreversible aqueous complexes are not considered. These equations are subject to the initial conditions

$$\Psi_j(0) = \Psi_j^0, \tag{39}$$

and

$$n_m(0) = n_m^0, \tag{40}$$

where Ψ_j^0 and n_m^0 designate the initial fluid and rock composition, respectively. A solution to these equations determines the solute concentrations $C_j(t)$ and mineral abundances $n_m(t)$ as functions of time t, and thus defines a reaction path parameterized by time. The path followed by the system depends on the specific form of the kinetic rate law used to describe the mineral reactions and on the initial conditions. The path begins from some initial state $\{\Psi_j^0,\ n_m^0\}$ and approaches the final state $\{\Psi_j^\infty,\ n_m^\infty\}$ as $t \rightarrow \infty$. Alternatively, the path of the system may be parameterized in terms of the reaction progress variable ξ which itself is a function of time. Because the system is closed, it is possible to represent the reaction rate as the total time derivative of the reaction progress variable $\xi_m(t)$ according to

$$I_m = \frac{d\xi_m}{dt}. \tag{41}$$

Thus it follows that

$$\Psi_j(t) = \Psi_j^0 - \sum_{m=1}^{M} \nu_{jm}\,\xi_m(t), \tag{42}$$

where the specific form of $\xi_m(t)$ depends on the reaction path.

By virtue of the fact that the system is closed, if the final state of the system is in thermodynamic equilibrium, it must be independent of the particular path the system takes to achieve equilibrium. In this case the final equilibrium state may be determined directly by algebraic equations alone, provided the assemblage of minerals in the final state is known, without solving complicated differential equations. To see this, note that the reaction rates may be eliminated from the first $N - M$ differential equations, by rearranging the order of the chemical species, if necessary, so that the square submatrix $\nu_{\bar{\alpha}m}$ with $\bar{\alpha} = N - M + 1,\ \cdots,\ N$ and $m = 1,\ \cdots,\ M$ is nonsingular. Writing the mass transfer equations for the primary species separately for the first set of $N - M$ species and the remaining M species according to

$$\frac{d\Psi_\alpha}{dt} = -\sum_{m=1}^{M} \nu_{\alpha m} I_m, \quad (\alpha = 1, \cdots,\ N - M), \tag{43}$$

and

$$\frac{d\Psi_{\bar{\alpha}}}{dt} = -\sum_{m=1}^{M} \nu_{\bar{\alpha}m} I_m. \quad (\bar{\alpha} = N - M + 1, \cdots,\ N), \tag{44}$$

and solving the second set of M equations for the M reaction rates I_m yields:

$$I_m = -\sum_{\bar{\alpha}=N-M+1}^{N} (\nu^{-1})_{m\bar{\alpha}} \frac{d\Psi_{\bar{\alpha}}}{dt}, \tag{45}$$

where $(\nu^{-1})_{m\bar{\alpha}}$ denotes the inverse matrix to $\nu_{\bar{\alpha}m}$. Substituting this expression for I_m into the first set of $N-M$ equations yields

$$\frac{d}{dt}\left\{\Psi_\alpha + \sum_{\bar{\alpha}=N-M+1}^{N} \tilde{\nu}_{\alpha\bar{\alpha}}\Psi_{\bar{\alpha}}\right\} = 0, \tag{46}$$

where $\nu_{\alpha\bar{\alpha}}$ is defined by the equation

$$\tilde{\nu}_{\alpha\bar{\alpha}} = -\sum_{m=1}^{M} \nu_{\alpha m}(\nu^{-1})_{m\bar{\alpha}}. \tag{47}$$

The quantity in curly brackets is conserved along the reaction path. Integrating this equation yields the result

$$\Psi_\alpha - \Psi_\alpha^0 + \sum_{\bar{\alpha}=N-M+1}^{N} \tilde{\nu}_{\alpha\bar{\alpha}}\left(\Psi_{\bar{\alpha}} - \Psi_{\bar{\alpha}}^0\right) = 0 \quad (\alpha = 1, \cdots, N-M). \tag{48}$$

These equations combined with M mass action equations corresponding to the minerals in the final equilibrium state provide N equations in N unknowns from which the final equilibrium state can be determined. As in the case of a closed system it is also possible to define conserved quantities for an open system. In this case the time derivative appearing in Eqn.(46) is replaced by the differential operator $\widehat{\mathcal{L}}$ defined by (Lichtner, 1991)

$$\widehat{\mathcal{L}} = \frac{\partial}{\partial t}\phi + \frac{\partial}{\partial x}\phi D\frac{\partial}{\partial x} - u\frac{\partial}{\partial x}. \tag{49}$$

This observation is useful in a local equilibrium formulation of mineral reaction rates based on the quasi-stationary state approximation (Lichtner, 1991).

3.2. Stationary States: Open Systems

The open system analogue to a closed system reaction path is a stationary state. The stationary state transport equations follow from the quasi-stationary state approximation. This approximation is rigorously based on the transient mass conservation equation, Eqn.(20), in which the term involving the partial time derivative of the solute concentration is neglected compared to the remaining terms (Lichtner, 1988). Thus it is assumed that

$$\frac{\partial}{\partial t}(\phi\Psi_j) \simeq 0, \tag{50}$$

and

$$\frac{\partial}{\partial t}(C_i) \simeq 0. \tag{51}$$

This results in a system of ordinary differential equations in the space coordinate alone in which time enters only as a parameter characterizing the state of alteration of the host rock. The resulting solution is referred to as a stationary state.

Retaining the diffusive and dispersive flux terms in Eqns.(23) and (9), the stationary state transport equations form a system of second order ordinary differential equations, given by

$$\left[-\phi D\frac{d^2}{dx^2}+u\frac{d}{dx}\right]\Psi_j(x,\,t)\;=\;-\sum_{m=1}^{M}\nu_{jm}^{kin}I_m(x,\,t), \tag{52}$$

for primary species, and

$$\left[-\phi D\frac{d^2}{dx^2}+u\frac{d}{dx}\right]C_i(x,\,t)\;=\;I_i^{kin}(x,\,t), \tag{53}$$

for irreversible aqueous complexes. Accordingly there are a total of $N+N_{kin}$ ordinary differential equations. For the case of pure advective transport the stationary state transport equations reduce to first order ordinary differential equations of the form

$$u\frac{d\Psi_j}{dx}(x,\,t)\;=\;-\sum_{m=1}^{M}\nu_{jm}I_m(x,\,t), \tag{54}$$

for primary species, and

$$u\frac{dC_i}{dx}(x,\,t)\;=\;I_i^{kin}(x,\,t), \tag{55}$$

for irreversible aqueous complexes. These latter equations, $N+N_{kin}$ in number, correspond to the solute transport equations solved by the code **MPATH**.

The pure advective stationary state transport equations are far easier to solve than the corresponding advection–diffusion, stationary state equations. The latter case requires solving a set of second order ordinary differential equations in the space coordinate. This requires specifying two boundary conditions, compared to one in the pure advective case. However, only one condition is usually known, namely the fluid composition at the inlet. The second condition can, generally, be obtained only by solving the transport equations themselves. One possibility is to impose a zero gradient boundary condition on the solute concentrations far from the inlet. In addition, because of the necessity to compute the spatial derivative of the solute concentration occurring in the diffusion term, a spatial grid must be defined before the calculation is begun. Because the sequence of mineral zones is not generally known before hand, the grid points are not adapted to the positions of the reaction zones. This is in contrast to the pure

advective case in which the spatial grid is generated as the solution to the differential equations is obtained, and thus is automatically adapted to the mineral zonation pattern. Therefore, in the case of transport involving diffusion the grid must be refined during successive iterations, if an accurate solution is to be obtained. While none of these problems present fundamental difficulties, they do significantly increase the computational effort required to solve the transport equations with diffusion present.

To account for the moving boundary aspects of the transport–reaction problem it is necessary to introduce a reaction index ζ_m as in the transient description. The reaction rate I_m consists of the product of the reaction index and the intrinsic reaction rate as defined by Eqn.(15). As the fluid packet traverses the flow path, the reaction status of a mineral may change as a consequence of several factors. A non-reacting mineral may become reacting if (1) the solution composition becomes super-saturated with respect to the mineral, or (2) the fluid packet comes in contact with the mineral at some point along the flow path. A reacting mineral may become non-reacting if (1) the fluid comes to equilibrium with respect to the mineral, or (2) the packet is no longer in contact with the mineral and the fluid is under-saturated with respect to the mineral.

For pure advective transport, only the Darcy flow velocity enters the stationary state transport equations and not the average fluid velocity which depends on the porosity of the porous medium. Thus as long as the porosity may be considered constant, it does not affect the behavior of the system. The reaction zone velocities and zone widths are all independent of the porosity for a constant porosity system (Lichtner et al., 1987). Furthermore, in the asymptotic limit of large times and for constant concentration boundary conditions given by Eqns.(27) and (28), the pure advective transport equations must yield solutions similar to the combined advection–diffusion/dispersion equations (Lichtner, 1992). This observation is based on the scaling properties of the mass transport equations (see Eqns.(73) and (74)). An additional requirement for the scaling relations to hold is that there is no inherent length scale associated with the problem. The main difference between the two solutions with and without diffusion present, is in the widths of the various reaction zones which differ by the characteristic diffusion length of the system after a sufficiently long time span. However all other properties such as the the reaction zone sequence, reaction front velocities, solute concentrations and mineral modal compositions should eventually be the same after sufficient time has elapsed.

By introducing the travel time t' of a fluid packet, related to the spatial coordinate x by the equation

$$x = vt', \tag{56}$$

where v denotes the average fluid velocity, related to the Darcy velocity by the porosity according to the expression

$$v = \frac{u}{\phi}, \tag{57}$$

the stationary state equations have the same form as the mass transfer equations describing reaction in a closed system. In fact reaction paths for open and closed systems are often very similar. The essential difference between the two systems is that in the open system product minerals are not able to back react with the fluid, but are deposited along the flow path and are no longer in contact with the fluid packet once formed. A common error in applying the open system, single reaction path model to a flowing fluid, is to attempt to calculate the change in porosity from the total volume change due to mineral reactions taking place along the entire flow path. This procedure forgets that mineral reaction products, and hence change in porosity, are distributed over the entire flow path and not at a single point. It is only by considering many reaction paths that mineral abundances and porosity can be calculated at a fixed point in space as a function of time. How this may be carried out within the multiple reaction path formulation is considered in the next section.

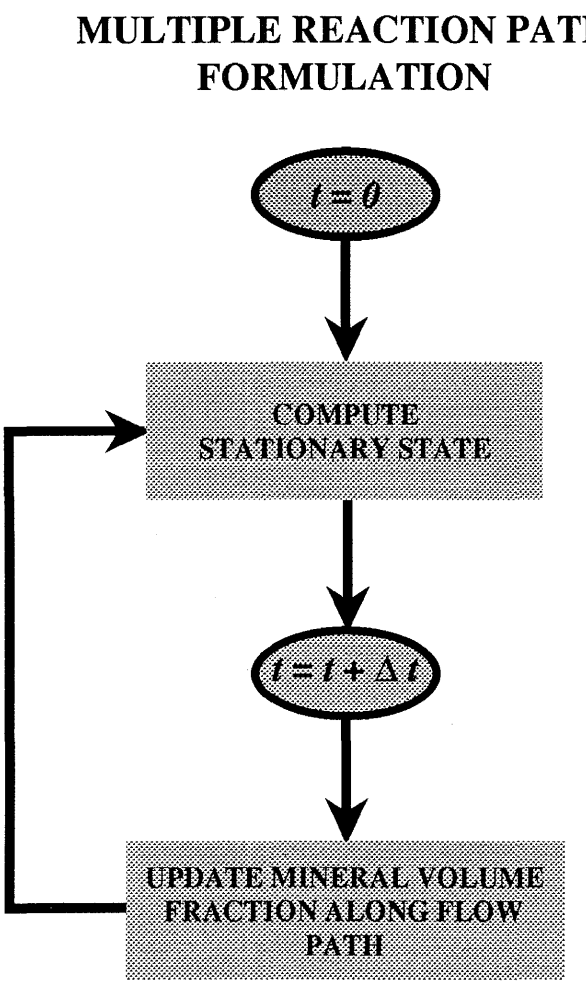

Figure 1: Schematic illustration of the multiple reaction path formulation of fluid transport and chemical reaction of minerals in a porous medium. With each time step Δt a new state of alteration of the host rock is obtained which determines a new stationary state.

3.3. Time Integration of Mineral Mass Transfer Equations

A single stationary state, or reaction path, describes the fluid composition as a function of distance along the flow path for a given state of alteration of the host rock. To obtain the time evolution of the system, a sequence of reaction paths must be considered with each path derived from the previous path through alteration of the host rock. While a single reaction path enables the fluid composition and mineral reaction rates to be calculated at each point along a streamline, many reaction paths are required to obtain the change in solute concentrations and mineral modal compositions with time at a fixed point in space. Once a reaction path has been obtained by

solving either Eqns.(52) and (53), or Eqns.(54) and (55) a new state of alteration of the host rock can be computed at each point along the flow path by integrating the mineral reaction rates according to Eqn.(10) over some time interval Δt. From the newly altered host rock, a new reaction path can be computed and so on. In this way the time evolution of a geochemical system is represented as a sequence of stationary states. The final result must, of course, be independent of the time step Δt between reaction paths. Choosing time steps too small results in prohibitively time consuming computations. If the time step is too large, however, convergence of the solution is not obtained. For the multiple reaction path formulation to be useful it is necessary that the solute concentration becomes stationary in time much more rapidly than the duration of a single stationary state represented by the time step Δt. A schematic illustration of the multiple reaction path formulation as implemented in **MPATH** is shown in Fig. 1.

Integrating Eqn.(10) over the time interval Δt_k, the mineral volume fraction $\phi_m^k(x)$ at a fixed position x along the flow path is obtained at time t_k according to the equation

$$\phi_m^k(x) \;=\; \phi_m^{k-1}(x) + \Delta t_k\, \bar{V}_m\, I_m^k(x), \tag{58}$$

where

$$\Delta t_k \;=\; t_k - t_{k-1}, \tag{59}$$

for $k = 1, 2, \cdots$, with $t_0 = 0$. This expression gives the volume fraction of the mth mineral in terms of the mineral reaction rate $I_m^k(x)$ obtained from the stationary state $\Psi_j^k(x)$, and the volume fraction corresponding to the state of alteration of the host rock at time t_{k-1}. The first stationary state ($k = 1$) results from reaction of a fluid packet with the unaltered host rock, represented by ϕ_m^0, corresponding to Helgeson's single reaction path. With the newly obtained distribution of minerals obtained from Eqn.(58), a new stationary state can be calculated and so on, resulting in the sequence of stationary states $\{\Psi_j^1, \Psi_j^2, \cdots, \Psi_j^k, \cdots\}$ corresponding to the times $t_1, t_2, \cdots, t_k, \cdots$. The kth stationary state may be thought of having a lifetime Δt_k during which the altered rock profile is transformed from ϕ_m^{k-1} to ϕ_m^k. Symbolically this process may be represented as:

$$\phi_m^{k-1} \rightarrow \Psi_j^k \overset{\Delta t_k}{\rightarrow} \phi_m^k. \tag{60}$$

The quasi-stationary state approximation assumes that the transient period during which the fluid composition establishes a stationary state can be completely neglected. Because the stationary

transport equations, Eqns.(54) and (55), are solved independently of Eqn.(10), the problem is greatly simplified.

Equation (58) is not completely correct for times t for which the fluid packet has not yet traversed the entire flow path, or if the fluid packet does not reach equilibrium with the host rock within a distance much less than $v\Delta t$. In either of these cases it is necessary to take into account the finite travel velocity of the packet. In time t the fluid packet travels a distance vt. For $vt < L$, for a flow path of length L, the host rock remains unaltered for $x > vt$. For the very first stationary state with assumed lifetime Δt_1, the contact time of the packet with the host rock for $x < L$, is $\Delta t - v/x$, which varies with distance and becomes zero at $x = vt$. The mineral volume fraction at time $t = \Delta t_1$, corresponding to the first stationary state is thus given by

$$\phi_m^1(x) = \phi_m^0 + \left(\Delta t_1 - \frac{x}{v}\right) \bar{V}_m I_m [1 - \theta(x - v\Delta t_1)]. \tag{61}$$

For the general case corresponding to the kth stationary state, integrating Eqn.(10) from t_{k-1} to t_k results in the expression

$$\begin{aligned} \phi_m^k(x) = \phi_m^{k-1}(x) + \bar{V}_m I_m^k(x) \Big\{ & \Delta t_k [1 - \theta(x - vt_{k-1})] \\ & + \left(t_k - \frac{x}{v}\right) [\theta(x - vt_{k-1}) - \theta(x - vt_k)] \Big\}. \end{aligned} \tag{62}$$

This equation is illustrated in the time–distance diagram in Fig. 2. For the example shown, two time steps are required for the fluid packet to completely traverse the total length of the flow path L with $L = 2v\Delta t$. For the first two steps the contact time of the packet varies with distance along the flow path given by the triangular regions. For the general case in which n steps are required to traverse the flow path, as long as $n\Delta t$ is sufficiently small compared to the time required to cause substantial alteration of the host rock, this time period is not expected to significantly alter the final results. With increasing time the correction terms in Eqn.(62) become less and less important, until the entire length of the host rock has been infiltrated at which time Eqn.(58) applies. Strictly speaking the quasi–stationary state approximation is only valid if the fluid packet comes to equilibrium with the host rock over a travel distance much less than $v\Delta t$, the distance the fluid is displaced during one time step. If this is not the case, transient effects are introduced which are not accounted for in this approximate treatment. However in most cases such effects are not expected to introduce a substantial error.

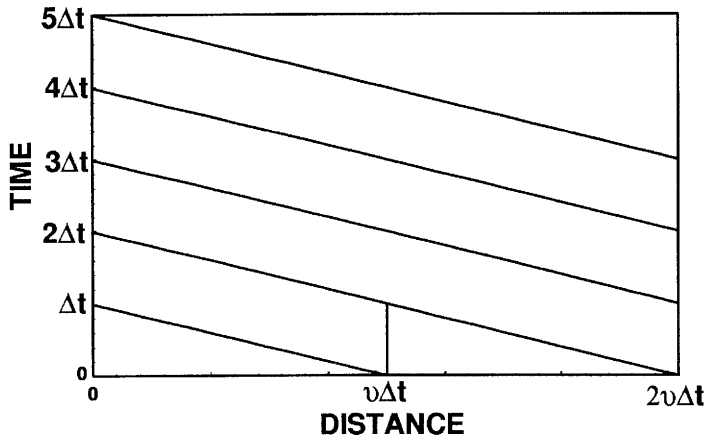

Figure 2: Time–distance diagram illustrating integration of the mineral mass transfer equations.

4. NUMERICAL SOLUTION

The only case where an analytical solution is known to the transport equations with moving boundaries and kinetic reaction of minerals is a single component system with linear kinetics [Lichtner, 1988, 1992]. In general, the transport equations must be solved numerically. These equations present special numerical difficulties because of their mathematical stiffness, resulting from the wide range of values for the kinetic rate constants often spanning many orders of magnitude. Redox reactions introduce additional difficulties often leading to extremely sharp reaction fronts.

4.1. The Code MPATH

The quasi–stationary state approximation, or multiple reaction path formulation of a time–space description of solute transport in a porous medium has been implemented in the numerical algorithm **MPATH**. The code **MPATH** is capable of describing two distinct types of physical processes: (1) a fluid packet moving with constant velocity forming an open system; and (2) batch reaction in a closed system. Additional features of **MPATH** include among others: distribution of species algorithm to determine the initial composition of the reacting fluid; efficient computation of reaction paths with an adaptive time step algorithm which adjusts to

local features of the path; a flexible data base format is included with the program, providing for porting of the EQ3/6 (Wolery, 1987) data base and SUPCRT (Johnson et al., 1991) generated data bases; irreversible precipitation and dissolution of minerals; disequilibrium of aqueous complexes including redox couples; and various prescribed temperature profiles which may vary with time and distance.

The **EQ3/6** data base contains an extensive set of minerals and aqueous species including over 1500 aqueous species and minerals. Log K values are stored at a grid of temperatures corresponding to 0, 25, 60, 100, 150, 200, 250 and 300°C at fixed pressures lying along the steam saturation curve. Other data bases can be easily generated using **SUPCRT92** for any desired temperature–pressure conditions specific to the problem at hand. The temperature dependence of the equilibrium constants is interpolated according to the expression

$$\log K = \frac{a_{-2}}{T^2} + \frac{a_{-1}}{T} + a_0 \ln T + a_1 + a_2 T, \tag{63}$$

where T denotes the absolute temperature in degrees Kelvin, and the coefficients a_i are fit parameters. An equation of state for pure water derived from Haar et al. [1980] is used by **MPATH**.

The user must select which minerals to include in the calculation for the particular geochemical system considered. This cannot be predicted by theory alone and often requires some subjective criteria on the part of the user. Some idea of which secondary minerals to include can be obtained by checking the saturation indices to determine which minerals might be likely candidates to precipitate. Certain minerals, however, only nucleate at sufficiently high temperatures and for calculations involving low temperatures, such as weathering, can be eliminated on that basis even if their saturation indices suggest they should form. An additional factor that must be taken into account is the existence of nucleation kinetics which commonly results in the presence of a kinetic barrier prohibiting reaction, even if thermodynamically feasible. An option in the code allows minerals to remain super-saturated without reacting until a specified threshold affinity is reached.

Activity coefficient corrections are calculated using an extended Debye–Hückel algorithm

$$\log \gamma_l = \frac{-z_l^2 A \sqrt{I}}{1 + B\mathring{a}_l \sqrt{I}} + \dot{b} I, \tag{64}$$

where A, B, $\mathring{a}_l$ and $\dot{b}$ are constants, z_l denotes the valence of the lth species and I denotes the ionic strength of the aqueous solution defined by

$$I = \frac{1}{2}\sum_{j=1}^{N} z_j^2 m_j + \frac{1}{2}\sum_{i=1}^{N_{rev}} z_i^2 m_i^{rev} + \frac{1}{2}\sum_{l=1}^{N_{kin}} z_l^2 m_l^{kin}, \tag{65}$$

where m_j, m_i^{rev} and m_l^{kin} denote the molalities of the subscripted species. Molality is related to concentration by the approximate equation

$$\rho_0 m_j = C_j, \tag{66}$$

and similarly for aqueous complexes, where ρ_0 denotes the density of pure water at the temperature and pressure of interest.

Redox reactions are incorporated in **MPATH** in terms of actual species in solution, rather than a hypothetical electron. This guarantees conservation of electrons in the overall oxidation–reduction reaction. Because of the sudden changes in concentration associated with some oxidation–reduction reactions, it is crucial to solve the finite difference residual functions for the logarithm of the solute concentration, rather than the concentration itself. This enables a numerically stable solution to be obtained for any fixed set of primary species along the entire flow path. If the concentration is used, then it is necessary to use basis switching to ensure that only the dominant primary species are used when solving the residual equations. The transformation of the field variables Ψ_j, Ω_j and the stoichiometric coefficients ν_{ji}^{rev}, ν_{il}^{kin} and ν_{jm} to a different choice of primary species is given in Appendix B. The code itself choses the dominant redox couple, which may change along the flow path according to solution concentrations and redox state. Thus, for example, as the fluid packet crosses a redox front and the oxygen fugacity plummets towards zero, some species other than $O_{2(aq)}$ is chosen to represent the oxidation state of the fluid. Before the fluid packet reaches the redox front, large steps can be taken but, as the redox front is crossed, extremely short steps are required because of the rapidly changing concentrations of redox sensitive species across the front. A similar situation is encountered in hydrolytic fronts, but on a much smoother length scale, with pH-dependent species such as aluminum. In addition, an efficient adaptive step size algorithm for advancing the solution along a streamline is essential. The step size must be allowed to both increase or decrease as smooth or rapid changes in concentration are encountered along the flow path. Consider, for example, a fluid packet as it crosses a redox front and the oxygen

fugacity plummets towards zero. Before the fluid packet reaches the redox front large steps can be taken, but as the redox front is crossed extremely short steps are required because of the rapidly changing concentrations of redox sensitive species across the front. A similar situation is encountered in hydrolytic fronts with pH-dependent species such as aluminum, but over a much smoother length scale. An adaptive grid algorithm similar to that presented by Press et al. [1987] is used in **MPATH**.

Integrating the mineral mass transfer equations requires introducing a spatial grid at which to store the mineral volume fractions. This is accomplished by using the same node points at which the stationary state solute transport equations are solved, which are automatically determined as part of the solution, thereby associating a spatial grid network with each stationary state. This defines a moving grid which changes with each stationary state. The grid points are closely adapted to the particular sequence of reaction zones which are determined by the current state of alteration of the host rock. The volume fractions calculated at node points corresponding to the previous stationary state, are interpolated to the new node points of the current stationary state to carry out the integration. In this way reaction fronts can be tracked with time and extremely narrow reaction zones easily resolved to any desired accuracy.

Irreversible reactions require specification of a kinetic rate law and allow parameterization of the reaction path as an explicit function of the time that a mineral is in contact with the aqueous solution. The time coordinate may be interpreted either as the time corresponding to a closed system batch process, or as representing the travel time of a packet of fluid undergoing pure advective transport. In the latter, open system case, the travel time may be converted to the distance of travel of the packet along a streamline by multiplying by the flow velocity in a Lagrangian representation. This interpretation is based on the quasi-stationary state approximation (Lichtner, 1988). The distinction between these two processes is important to keep in mind when interpreting the results of a particular calculation. Thus the amount of a mineral precipitated or dissolved has a different meaning: in the batch process it refers to the actual amount of each mineral produced or destroyed within the container; whereas in the open system process it refers to minerals distributed along the entire flow path. In the open system case the contribution to the mineral abundance at a fixed point in space from the passage of a single packet of fluid is usually very small in most circumstances.

4.2. Newton-Raphson Equations

In the routine **MPATH** the stationary state solute transport equations for pure advective transport are solved numerically using an implicit finite-difference algorithm. The residual functions for primary species are given by the equation

$$R_j = \Psi_j(x+\Delta x) - \Psi_j(x) + \frac{\Delta x}{u} \sum_{m=1}^{M} \nu_{jm} \left(\lambda I_m(x+\Delta x) + (1-\lambda) I_m(x)\right), \qquad (67)$$

and, for irreversible aqueous complexes, by

$$R_l = C_l(x+\Delta x) - C_l(x) - \frac{\Delta x}{u} \left(\lambda I_l^{kin}(x+\Delta x) + (1-\lambda) I_l^{kin}(x)\right), \qquad (68)$$

for a step size Δx. The quantity λ controls the type of finite-difference method. The value $\lambda = 0$ results in an explicit finite-difference algorithm which becomes unstable for Δx too large, whereas $\lambda = 1$ is a fully implicit backward method and is unconditionally stable. For systems of equations involving chemical reactions, the implicit approach is preferred because of the stiff nature of the equations. These equations represent a set of $N + N_{kin}$ nonlinear algebraic equations to determine the concentrations of the primary species at position $x + \Delta x$ in the column. They are solved using a Newton–Raphson approach. The linearized residual equations are given by

$$\sum_{n'=1}^{N+N_{kin}} \mathcal{J}^{\iota}_{nn'} (y^{\iota+1}_{n'} - y^{\iota}_{n'}) = -R^{\iota}_{n}, \qquad (69)$$

where the Jacobian matrix $\mathcal{J}_{nn'}$ is defined by

$$\mathcal{J}_{nn'} = \frac{\partial R_n}{\partial y_{n'}}, \qquad (70)$$

and the variables $\{y_n\}$ refer to the unknown solute concentrations $\{C_1, \cdots, C_N, C_1, \cdots, C_{N_{kin}}\}$. Explicit expressions for the partial derivatives appearing in the definition of the Jacobian are given in Appendix C.

4.3. Numerical Accuracy

When integrating the transport equations over the extremely long time spans which characterize many natural geochemical systems it is important to have some means to test the solution for its accuracy. Cumulative numerical round off errors, for example, could render the solution

meaningless. Therefore in the code **MPATH** global mass conservation conditions are verified for each stationary state by evaluating the integrated form of the transport equations. Defining

$$\Phi_m(t) \;=\; \int_0^L \phi_m(x,\, t)\, dx, \tag{71}$$

where L denotes the total length of the system, it follows that the following identity must hold:

$$u\left[\int_0^t \Psi_j(L,\, t')\, dt' - \Psi_j^0\, t\right] \;=\; -\sum_{m=1}^{M} \nu_{jm}\, \bar{V}_m^{-1}\, \left(\Phi_m(t) - \Phi_m^0\right). \tag{72}$$

The left hand side of the equation corresponds to the difference in the total amount of the jth primary species leaving and entering system, whereas the right hand side denotes the total amount that is stored in minerals over the entire flow path. This equation does not allow any statement to be made about the spatial accuracy of the solution, however. For elements such as uranium or copper, which may become trapped at redox fronts and therefore never leave the system, both the left and right hand sides of this equation must vanish separately if their inlet concentration is zero. In this case the element is recycled within mineral phases and the system is effectively closed with respect to such species.

There exists another important test of the accuracy of the asymptotic form of the kinetic solution for certain cases for which a corresponding local equilibrium solution exists. For the case of constant concentration boundary conditions the solution to the mass transport equations describing advection and diffusion of solute species in a homogeneous porous medium satisfies the scaling relation (Lichtner, 1992):

$$\mathcal{F}(\sigma x,\, \sigma t;\, \{k\},\, D,\, u) \;=\; \mathcal{F}(x,\, t;\, \sigma\{k\},\, \sigma^{-1} D,\, u), \tag{73}$$

where the quantity $\mathcal{F}(x,\, t;\, \{k\},\, D,\, u)$ refers collectively to the field variables concentration and mineral volume fraction, and σ is any real number. The dependence on the independent variables x and t and the parameters $\{k\}$, D and u is indicated explicitly. The notation $\{k\}$ refers to the set of kinetic rate constants $\{k_1,\, k_2,\, \cdots\}$, with $\sigma\{k\} = \{\sigma k_1,\, \sigma k_2,\, \cdots\}$. For the scaling relations to apply, it is necessary that there does not exist any externally imposed length scale, such as the position of a water table or temperature gradient. The reader is referred to Lichtner (1992) for more details.

The scaling relation is useful for obtaining the asymptotic properties of the system for long time spans and provides a means of testing the numerical accuracy of the kinetic solution. In the

limit $\sigma \rightarrow \infty$, the right hand side of Eqn.(73) approaches the pure advective local equilibrium limit and thus

$$\lim_{\sigma \rightarrow \infty} \mathcal{F}(\sigma x, \sigma t; \{k\}, D, u) = \mathcal{F}^{leq}(x, t; u), \tag{74}$$

where $\mathcal{F}^{leq}(x, t; u)$ denotes the local equilibrium solution corresponding to pure advective transport. Thus for sufficiently long time spans the solution to the kinetic mass transport equations is scalable to the local equilibrium solution for pure advective transport. This result was noted previously by Lichtner (1992). Because the local equilibrium solution is obtained by solving a system of non-linear algebraic equations (Walsh et al., 1984; Lichtner, 1991), it does not suffer from the possible effects of cumulative roundoff errors as does the kinetic solution. Unfortunately a local equilibrium solution may not always exist, or may be difficult to find due to the difficulty in determining the reaction zone sequence and due to the presence of so-called ghost zones (Schechter et al., 1987; Lichtner, 1992; Lichtner and Balashov, 1992; Lichtner and Waber, 1992). The width of a ghost zone is proportional to the characteristic diffusion length of the system and vanishes in the limit of pure advective transport for conditions of local chemical equilibrium, as discussed by Lichtner and Balashov (1992). Its name comes from the property that for pure advective transport under conditions of local equilibrium the width of a ghost zone vanishes; nevertheless, the fluid composition downstream from the zone remains in equilibrium with the minerals in the zone. Ghost zones exhibit the peculiar property that their width decreases with increasing fluid velocity.

Although the code **MPATH** is restricted to pure advective transport, according to the above scaling relation, for sufficiently long time spans this does not appear to be as drastic a simplification as might at first be thought. Only the widths and shapes of the mineral abundance profiles are different. Instead of the sharp fronts that occur in a local equilibrium description, rounded corners of the mineral profiles occur in the kinetic description. The reaction front velocities, mineral abundances and solute concentrations all approach their local equilibrium counterparts provided such solutions exist. Only for sufficiently early times can substantial differences exist between kinetic and local equilibrium solutions, with the exception of ghost zones whose widths are also determined by diffusive transport.

5. EXAMPLES

In the following, several examples are considered using the computer code **MPATH**. These examples illustrate the necessity of integrating the governing equations over geologic time spans in order to describe the complete behavior of the system. Unless stated otherwise, all thermodynamic data used in the calculations are taken from the EQ3/6 data base [Wolery, 1987].

5.1. Single Component System

To illustrate the basic features of the code **MPATH** the simplest possible nontrivial example is considered, that of reaction in a single component system. An analytical solution to this problem exists within the quasi-stationary state approximation assuming constant porosity, permeability and mineral surface area. This example has been described extensively by Lichtner (1988, 1991, 1992).

As a fluid under-saturated with respect to a solid phase infiltrates into a porous column containing the solid, the solid dissolves producing a reaction front $l(t)$ which advances with time in the direction of flow. The problem is to determine the position of the dissolution front as a function of time and the concentration profile of the solute species and modal composition of the solid as functions of time and distance. The transport equations take the form

$$u\frac{dC}{dx} = -ks\,(C - C_{eq})\,\vartheta(x - l(t)), \tag{75}$$

for the solute species, and

$$\frac{\partial \phi_s}{\partial t} = ks\bar{V}_s(C - C_{eq})\,\vartheta(x - l(t)), \tag{76}$$

for the solid phase, where C denotes the solute concentration, k the kinetic rate constant, s the surface area per unit bulk volume of porous medium, C_{eq} the equilibrium concentration, and ϕ_s and $\bar{V}_s$ denote the volume fraction and molar volume of the solid phase, respectively. The reaction index ζ_s may be expressed in terms of the Heaviside function $\vartheta(x)$, equal to one if $x \geq 0$, and zero otherwise. These equations are solved subject to the initial and boundary conditions

$$C(0, t) = C_0, \tag{77}$$

and

$$\phi_s(x,\,0) \;=\; \phi_s^{\infty}, \tag{78}$$

specifying the inlet fluid composition and initial solid volume fraction, respectively. In addition the solute concentration must be continuous across the reaction front $l(t)$.

The moving boundary problem posed by these equations requires determining the solute concentration $C(x,\,t)$, mineral volume fraction $\phi_s(x,\,t)$ and position of the dissolution front $l(t)$. The solute concentration can be expressed in the form

$$C(x,\,t) \;=\; [1-\vartheta(x-l(t))]\;C_0 + \left[C_{eq} - (C_{eq}-C_0)\;\mathrm{e}^{-q(x-l(t))}\right]\;\vartheta(x-l(t)), \tag{79}$$

where the inverse length q is defined by the equation

$$q \;=\; ks/u. \tag{80}$$

This result is obtained by solving Eqn.(75) separately for the two regions $x \leq l(t)$ and $x \geq l(t)$ and matching the solutions at the reaction front. As shown by Lichtner (1988) the mineral volume fraction satisfies the expression

$$\phi_s(x,\,t) \;=\; \phi_s^{\infty}\;\left[1-\mathrm{e}^{-q(x-l(t))}\right]\;\vartheta(x-l(t)). \tag{81}$$

The equation of motion satisfied by the dissolution front $l(t)$ can be determined by substituting Eqn.(81) into Eqn.(76) to give

$$v_l \;=\; \frac{dl}{dt} \;=\; \frac{1}{q\tau_0}, \tag{82}$$

where τ_0 denotes the time for the solid to completely dissolve at the inlet, given by

$$\tau_0 \;=\; \frac{\phi_s^{\infty}\,\bar{V}_s^{-1}}{ks(C_{eq}-C_0)}. \tag{83}$$

Note that the velocity of the front is independent of the kinetic rate constant and the porosity of the porous medium.

As noted by Lichtner (1988) the front velocity can be rewritten in the form

$$v_l \;=\; \frac{v}{K_{\Delta}}, \tag{84}$$

where v denotes the average fluid velocity defined in Eqn.(57) and where the quantity K_{Δ} is identical to the local equilibrium distribution coefficient for pure advective transport defined by

$$K_{\Delta} \;=\; \frac{\phi_s^{\infty}\bar{V}_s^{-1}}{\phi(C_{eq}-C_0)}. \tag{85}$$

The distribution coefficient K_Δ gives the ratio of solid to aqueous concentration of the solute species and is identical to the retardation coefficient for values much greater than one. Thus for pure advective transport the front velocity is constant and identical to the local equilibrium result. This statement is also true for transport by diffusion as demonstrated by Lichtner (1988). An explicit expression may be obtained for the position of the reaction front $l(t)$ by integrating Eqn.(82) subject to the initial condition

$$l(\tau_0) \;=\; 0. \tag{86}$$

This gives the following result valid for $t \geq \tau_0$ for pure advective transport for the position of the solid dissolution front $l(t)$ given by

$$l(t) \;=\; \frac{v}{K_\Delta}(t-\tau_0)\,\vartheta(t-\tau_0). \tag{87}$$

According to this equation, the dissolution front does not appear until $t > \tau_0$. For times earlier than this the solid is present over the entire flow path and dissolution occurs without movement of a reaction front. By contrast, in a local equilibrium description, a dissolution front is formed immediately as the inlet fluid begins to react with the solid.

In Fig. 3 the solute concentration, volume fraction and reaction rate are plotted as functions of distance for an elapsed time of 2000 years. The calculations assume values of $C_0 = 2 \times 10^{-3}$ moles liter^{-1}, $C_{eq} = 10^{-2}$ moles liter^{-1}, $u = 1$ m y^{-1}, $ks = 10^{-10}$ moles cm^{-3} sec^{-1} and $\phi_s^0 = 0.5$. For these values $\tau_0 \simeq 900$ years, and the retardation factor $K_\Delta \simeq 2.8 \times 10^4$. The essential difference between the kinetic and local equilibrium solutions lies in the behavior of the solute concentration and mineral volume fraction in the neighborhood of the dissolution front. In the case of local equilibrium jump discontinuities occur in these quantities at the front, in contrast to the smooth change obtained in the kinetic case. Furthermore the local equilibrium reaction rate is proportional to a delta function singularity. However, the velocity of the reaction front is the same for both cases regardless of the value of kinetic rate constant used in the calculation.

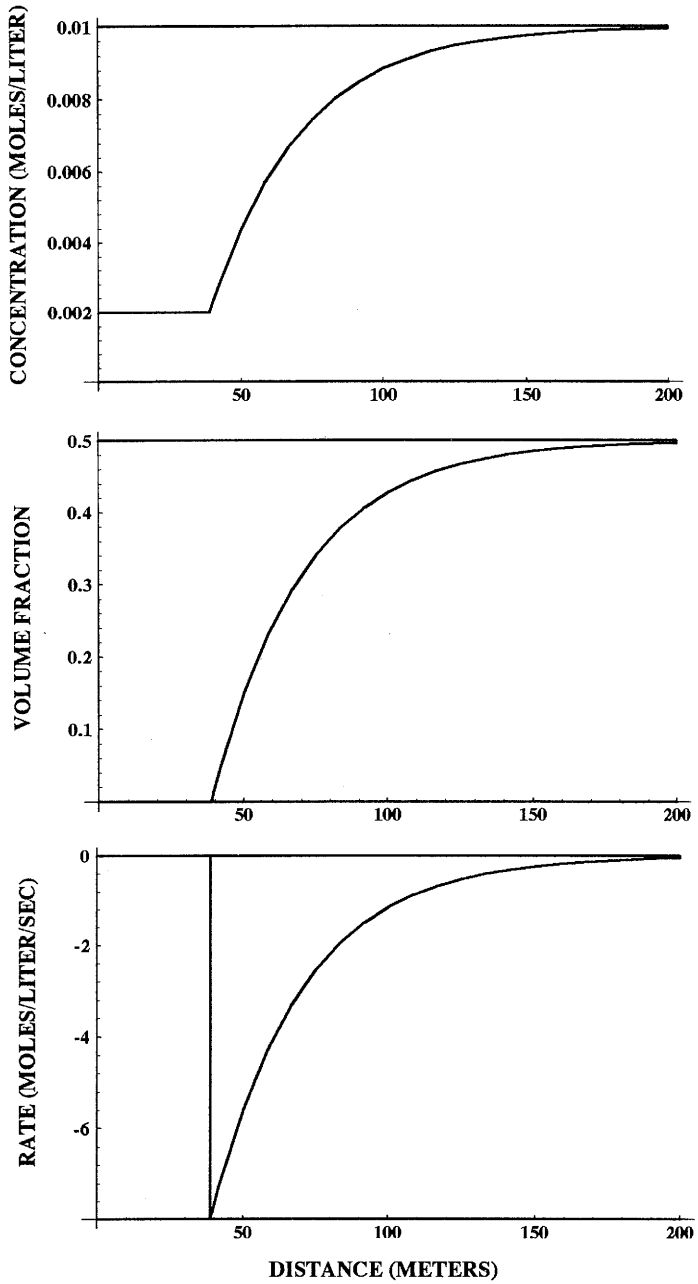

Figure 3: The solute concentration, solid volume fraction and reaction rate for a single component system plotted as a function of distance for an elapsed time of 2,000 years with the parameters given in the text.

5.2. Redox Problems

Redox problems can present special difficulties because of the extremely sharp nature of some redox fronts, marking the transition from oxidizing to reducing conditions. This is a consequence

of the large magnitude of the equilibrium constant associated with these reactions. Applications of **MPATH** to redox problems can be found in Lichtner and Waber (1992) describing the oxidation of pyrite and transport of uranium at the Osamu Utsumi uranium mine, Poços de Caldas, Brazil, and Lichtner and Biino (1992) describing supergene enrichment of a porphyry copper deposit.

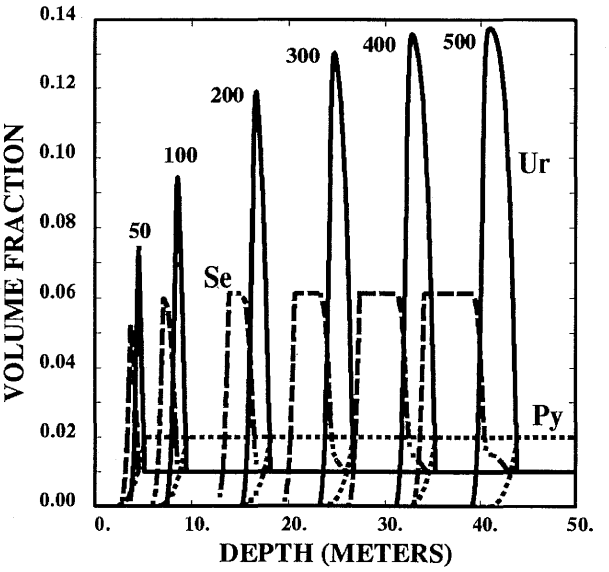

Figure 4: Volume fractions of uraninite (solid curves), native selenium (dashed curves) and pyrite (dotted curves) plotted as functions of distance for the indicated times in units of thousands of years. The host rock contains initial quantities of pyrite (2%), uraninite (1%) and native selenium (1%) by volume. Abbreviations used in the figure are: pyrite (Py), uraninite (Ur), and selenium (Se).

Here the relatively simple system consisting of pyrite (FeS_2), uraninite ($UO_{2(s)}$) and native selenium ($Se_{(s)}$) is considered in the absence of gangue minerals. Oxidizing water in equilibrium with the atmosphere percolates through a permeable host rock containing pyrite, uraninite and native selenium releasing uranium and selenium species into solution which reprecipitate further downstream. This process results in the supergene enrichment of these minerals in narrow zones at the top of the weathering column. This is shown in Fig. 4 where the volume fractions of pyrite, uraninite and native selenium are plotted as a function of distance for times ranging up to 500,000 years. The calculations are carried out for an inlet fluid in equilibrium with the atmosphere with pH 6 and total concentrations of uranium and selenium of 10^{-8} moles

liter^{-1}, and sulfur and iron of 10^{-12} moles liter^{-1}. A Darcy fluid velocity of 1 m y^{-1} is used in the calculation. Effective kinetic rate constants, defined as the product of the rate constant and mineral surface area, were chosen arbitrarily with values of 5×10^{-15} moles cm^{-3} s^{-1} for uraninite and native selenium, 2×10^{-15} moles cm^{-3} s^{-1} for pyrite, and 1×10^{-15} moles cm^{-3} s^{-1} for ferrihydrite. As demonstrated below, for the long time spans of interest here, the results depend only weakly on the choice of kinetic rate constants and mineral surface areas. To carry out the calculation 10,000 stationary states are constructed with equal time steps of 50 years.

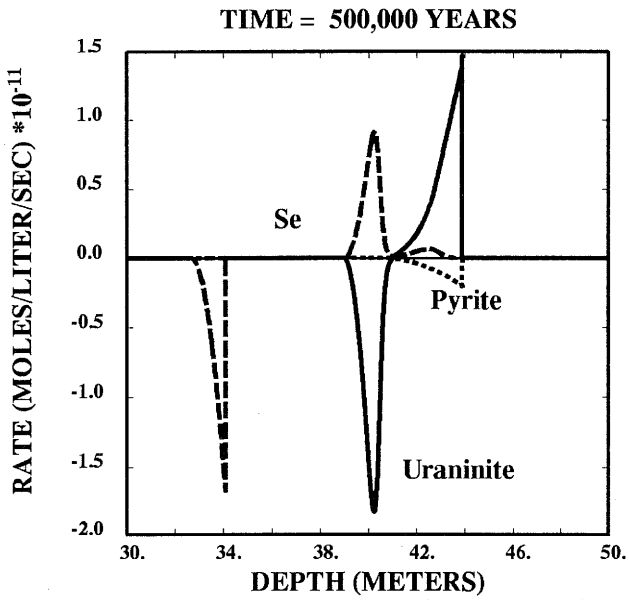

Figure 5: The reaction rates of uraninite (solid curves), native selenium (dashed curves) and pyrite (dotted curve) plotted as a function of distance for an elapsed time of 500,000 years for the same conditions as in the previous figure. A positive rate denotes precipitation and a negative rate dissolution. Both selenium and uraninite dissolve at their respective upstream boundaries as they become oxidized, and reprecipitate further downstream. Two peaks occur in the selenium precipitation rate.

For early times as the enrichment zones advance downward in the direction of the fluid, the maximum values in the uraninite and selenium volume fractions continuously increase with time. Eventually, however, after the zone widths become sufficiently wide, the fluid is able to reach equilibrium within the zones and a maximum volume fraction is obtained. The volume fraction for native selenium reaches a maximum value after approximately 100,000 years have elapsed, and after 400,000 years the uraninite volume fraction reaches its maximum value. For longer times the respective enrichment zones increase in width at constant modal composition.

The zone of enrichment for native selenium results in a bimodal distribution with a second plateau clearly visible after approximately 400,000 years have elapsed. A zone of ferrihydrite, not shown in the figure, forms initially but later disappears.

The reaction rates of native selenium, uraninite and pyrite corresponding to an elapsed time of 500,000 years are shown in Fig. 5 plotted as a function of distance. A positive rate denotes precipitation and a negative rate dissolution. Both selenium and uraninite dissolve at their respective upstream boundaries as they become oxidized, and reprecipitate further downstream, resulting in the downward displacement of the associated reaction zones. Two peaks occur in the selenium precipitation rate leading to the bi-modal volume fraction observed in the previous figure.

The reaction path of a fluid packet for an elapsed time of 500,000 years is shown in Fig. 6 plotted on a pe–pH activity diagram. The pe increases initially from the inlet value labeled by point A as selenium dissolves. The final point of the path labeled B is in equilibrium with pyrite. From this figure it is apparent that the bi-modal distribution in the selenium volume fraction results as the reaction path crosses the intersection of the stability lines of uraninite and selenium.

The pH, Eh and pe are plotted as functions of distance in Fig. 7 for the same time as the previous figure. Three distinct redox fronts are visible in the figure. The first corresponds to the oxidation front of native selenium occurring at approximately 34 meters from the inlet. The second redox front occurs at approximately 40 meters as uraninite is oxidized by selenium. At the third redox front located at a distance of 44 meters from the inlet pyrite becomes oxidized.

The pH drops sharply at the native selenium oxidation front and then remains constant until the uraninite oxidation front is encountered where it sharply rises. It drops again at the pyrite oxidation front. The positions of the selenium, uraninite and pyrite reaction fronts are marked by sharp changes in the concentrations of the appropriate solute species, as shown in Fig. 8 depicting the concentration profiles for selected aqueous species for the same time as in the previous figure.

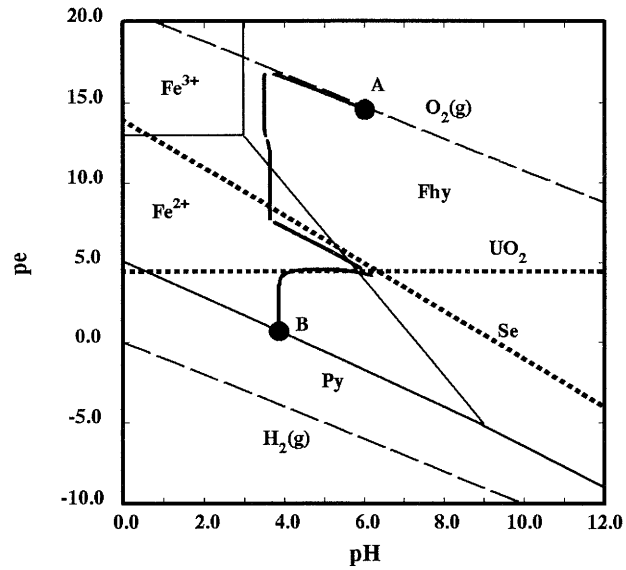

Figure 6: The reaction path of a fluid packet after an elapsed time of 500,000 years plotted on a pe–pH diagram. The point labeled A denotes the beginning of the path and the point B the final equilibrium state. The diagram is calculated based on the following constant activities: $\log a_{SO_4^{2-}} = -4$, $\log a_{UO_2^{2+}} = -5$, $\log a_{Fe^{2+}} = -4$, and $\log a_{SeO_3^{2-}} = -4$.

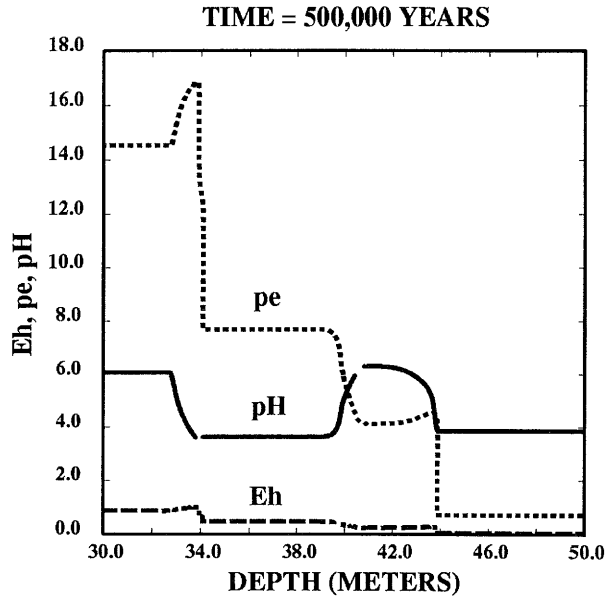

Figure 7: The pH, pe and Eh plotted as a function of distance for an elapsed time of 500,000 years for the same conditions as in the previous figure. See text for explanation of the calculated changes in pH across the different reaction fronts and the increase in pe as selenium is oxidized.

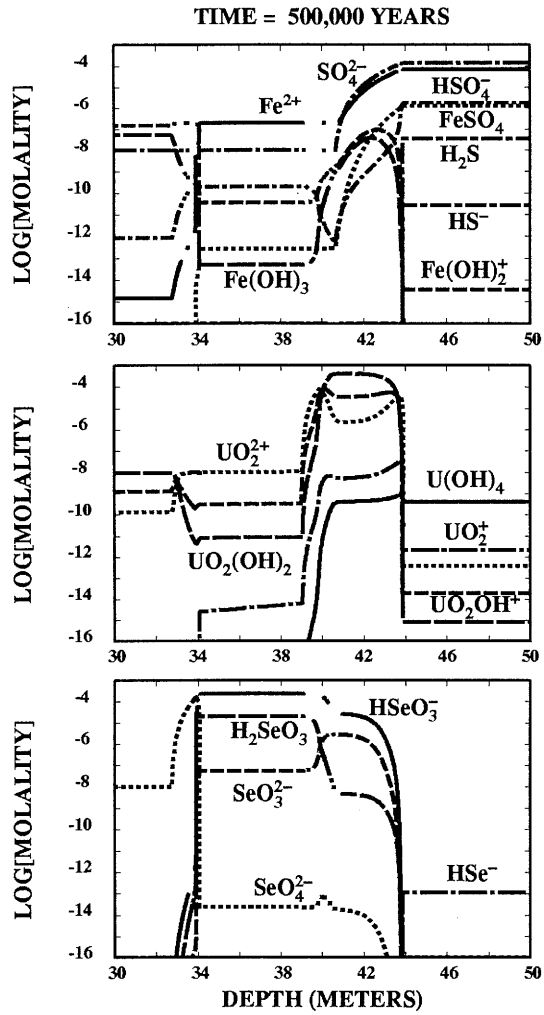

Figure 8: The profiles of selected aqueous species plotted as a function of distance for an elapsed time of 500,000 years for the same conditions as in the previous figure. The positions of the selenium, uraninite and pyrite reaction fronts are marked by sharp changes in the concentrations of the appropriate solute species.

Across the first redox front associated with the oxidation of native selenium, the dominant aqueous selenium species changes from selenate (SeO_4^{2-}) with a valence state of Se(VI), to hydrogen selenite ($HSeO_3^-$) with a valence state of Se(IV). The final valence state of selenium is Se(−II) in the form of hydrogen selenide HSe^-. Likewise uranium changes its oxidation state across the sequence of redox fronts from the U(VI) valence state to U(IV). Very large concentrations of selenium and uranium occur within the enrichment zone of selenium and uraninite. However, unlike sulfur and iron which are transported downstream in large concentrations,

both uranium and selenium are conserved within the enrichment zones and thus the system is effectively closed with respect to these elements.

To understand qualitatively the changes in pH and redox potential it is useful to construct approximate overall reactions at each of the reaction fronts. However, it must be emphasized that these reactions are only approximate representations of the actual reactions taking place in the system. At the upstream selenium front, selenium is oxidized by dissolved oxygen according to the approximate overall reaction:

$$Se_{(s)} + H_2O + 3/2O_2 \rightarrow SeO_4^{2-} + 2H^+, \tag{88}$$

with SeO_4^{2-} as the dominant selenium species. Dissolved oxygen is completely depleted from solution at this front. This reaction is consistent with the observed drops in the pH and pe as selenium is oxidized. Note, however, the *increase* in pe and Eh in Fig. 7 just before the dissolved oxygen concentration plummets to zero. This result is somewhat surprising since oxidation is usually associated with a *decrease* in the redox potential, according to the reaction

$$Se_{(s)} + 4H_2O \rightarrow SeO_4^{2-} + 8H^+ + 6e^-. \tag{89}$$

However, this reaction is only a half-reaction and is not the reaction that actually takes place at the oxidation front of selenium. To see how it is possible for the pe to increase with oxidation of $Se_{(s)}$, the oxygen fugacity is plotted in Fig. 9 as a function of distance along with the pe and pH. As can be seen from this figure, in the region where the pe increases, the pH decreases while the oxygen fugacity is essentially constant on a log scale. The oxygen fugacity, pe and pH are related by the reaction

$$e^- + H^+ + 1/4O_2 \rightleftharpoons 1/2H_2O. \tag{90}$$

Therefore, according to this reaction, if the pH drops while the oxygen fugacity remains approximately constant, the pe must increase, assuming that the activity of water may be considered constant, a good approximation for sufficiently dilute solutions. The questions remains as to why the oxygen fugacity is approximately constant as selenium begins to dissolve. Of course, the oxygen fugacity must decrease in accord with the reaction given in Eqn.(88). However, because the concentration of oxygen is initially large (in equilibrium with the atmosphere), and the initial concentration of hydrogen ions is relatively small (pH 6), the pH changes more rapidly than oxygen causing the pe to increase in accordance with the reaction in Eqn.(90). A similar

situation occurs at the third redox front where the pe also increases due to a drop in pH. In this case the oxygen fugacity has a negligibly small value.

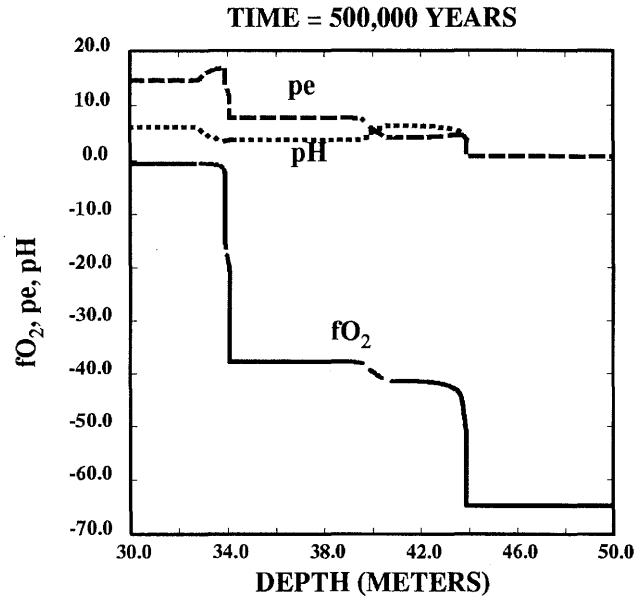

Figure 9: The oxygen fugacity f_{O_2}, pe and pH plotted as a function of distance for an elapsed time of 500,000 years for the same conditions as in the previous figure.

At the uraninite oxidation front the situation is more complicated. Here as uraninite dissolves as selenium precipitates. According to Fig. 7 the pH increases in the neighborhood of this front suggesting the approximate overall reaction:

$$2UO_{2(s)} + HSeO_3^- + 5H^+ \rightarrow Se_{(s)} + 2UO_2^{2+} + 3H_2O. \qquad (91)$$

This reaction is consistent with the calculated rates of uraninite dissolution and selenium precipitation with a ratio of 2:1 as shown in Fig. 5. According to this reaction selenium serves as the oxidant of uraninite.

At the third broader front, pyrite dissolves as both selenium and uraninite precipitate. At this front an approximate overall reaction consistent with the reaction rates shown in Fig. 5 with a ratio of 5:1 may be written in the form

$$FeS_{2(s)} + HSeO_3^- + 5UO_2^{2+} + 5H_2O \rightarrow Se_{(s)} + 5UO_{2(s)} + Fe^{2+} + 2SO_4^{2-} + 11H^+, \qquad (92)$$

corresponding to the second peak in the selenium precipitation rate. In this reaction both

selenium and uraninite act as oxidants of pyrite. According to this reaction the pH must decrease consistent with the results presented in Fig. 7.

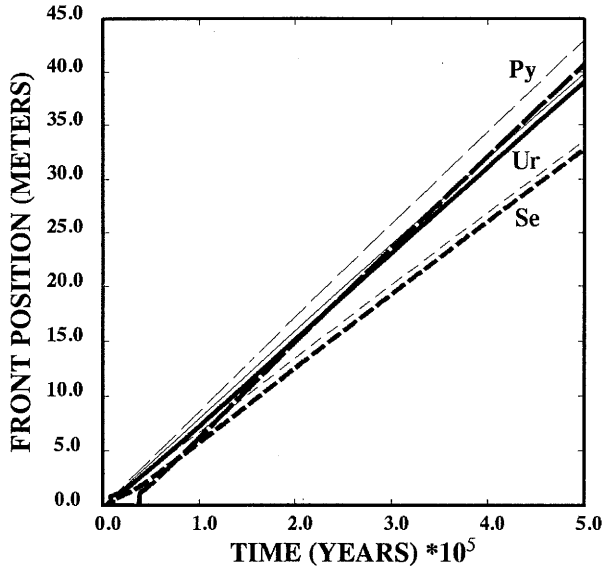

Figure 10: The positions of reaction fronts for pyrite (long dashed curve), uraninite (solid curve) and selenium (dashed curve) plotted as a function of time for the same conditions as in the previous figure. The corresponding thin lines refer to the local equilibrium calculation.

From the scaling properties of the transport equations (Lichtner, 1992), the maximum values obtained for the volume fractions are expected to agree with the corresponding local equilibrium result. That this is indeed the case may be demonstrated by comparing the results of the kinetic calculation with those obtained from the local equilibrium calculation presented in Table 1. The first column in the table gives the composition of the inlet fluid. Two alteration zones occur labeled zone 1 and zone 2, the first enriched in selenium and the second enriched in uraninite and only slightly enriched in selenium. The third zone refers to the unaltered protore containing pyrite, uraninite and selenium. The row labeled ϕ gives the porosity of the altered rock. The porosity of the unaltered rock is assumed to be 20%. The last row gives the velocity of the respective reaction fronts relative to the Darcy flow velocity u. As can be seen by comparison with the above figures the agreement between the local equilibrium and kinetic solutions for the solute concentrations and mineral volume fractions is excellent. Note that ferrihydrite does not

form in the local equilibrium calculation. Comparison with Figs. 7 and 8 further demonstrates excellent agreement between the pH, Eh and concentrations of aqueous species.

The kinetic calculation also yields the same values for the reaction front velocities, another general property of the scaling relations (Lichtner, 1992), as can be verified by comparing the slopes of the positions of the uraninite and selenium reaction fronts plotted in Fig. 10 with the local equilibrium results. The pyrite and uraninite fronts cross at approximately 250,000 years after which the zone sequence is in agreement with the local equilibrium result. As time increases a steady-state is achieved in which the reaction fronts propagate with constant velocity.

As can be seen from this example, for sufficiently long time spans the solution to the kinetic mass transport equations is, to a large extent, independent of the rate constants and mineral surface areas used in the calculation. With increasing time the solution becomes less and less dependent on kinetics. This is a very general observation that applies to all geochemical systems and is not limited to redox reactions.

Table 1: Results of a local equilibrium calculation for the oxidation of a pyrite bearing host rock containing uraninite and native selenium for the same initial and boundary conditions used in the kinetic calculation presented in Figs. 4–8.

	inlet	zone 1	zone 2	zone 3
pH	6.00	3.64	6.31	3.85
Eh	0.864	0.455	0.243	0.043
log P_{O_2}	−0.699	−37.8	−41.4	−64.8
	primary species			
Fe^{2+}	2.08×10^{-15}	2.22×10^{-7}	2.18×10^{-7}	7.11×10^{-5}
SO_4^{2-}	2.00×10^{-5}	1.96×10^{-5}	2.00×10^{-5}	1.61×10^{-4}
UO_2^{2+}	1.87×10^{-10}	9.56×10^{-9}	2.25×10^{-6}	3.94×10^{-13}
SeO_4^{2-}	1.00×10^{-8}	2.37×10^{-14}	1.77×10^{-14}	2.08×10^{-54}
	total concentrations			
Fe^{2+}	2.22×10^{-7}	2.22×10^{-7}	2.22×10^{-7}	7.25×10^{-5}
SO_4^{2-}	2.00×10^{-5}	2.00×10^{-5}	2.00×10^{-5}	1.65×10^{-4}
UO_2^{2+}	1.00×10^{-8}	1.00×10^{-8}	4.50×10^{-4}	4.11×10^{-10}
SeO_4^{2-}	1.00×10^{-8}	2.53×10^{-4}	2.79×10^{-5}	1.97×10^{-13}
	aqueous complexes			
HSO_4^-	1.86×10^{-9}	4.05×10^{-7}	9.13×10^{-10}	1.98×10^{-6}
HS^-	0.	0.	0.	2.63×10^{-11}
$H_2S_{(aq)}$	0.	0.	0.	3.48×10^{-8}
$FeSO_{4(aq)}$	6.22×10^{-18}	5.92×10^{-10}	6.35×10^{-10}	1.47×10^{-6}
$Fe(OH)_2^+$	1.70×10^{-7}	4.01×10^{-11}	2.32×10^{-9}	3.67×10^{-15}
$Fe(OH)_{3(aq)}$	5.28×10^{-8}	5.39×10^{-14}	1.46×10^{-9}	8.05×10^{-18}
UO_2^+	1.40×10^{-23}	5.70×10^{-15}	5.15×10^{-9}	2.12×10^{-12}
$U(OH)_{4(aq)}$	3.59×10^{-35}	1.20×10^{-19}	4.08×10^{-10}	4.08×10^{-10}
UO_2OH^+	1.13×10^{-9}	2.44×10^{-10}	2.73×10^{-5}	1.62×10^{-14}
$UO_2(OH)_{2(aq)}$	8.66×10^{-9}	8.02×10^{-12}	4.20×10^{-4}	8.66×10^{-16}
$UO_2(OH)_3^-$	1.10×10^{-11}	4.49×10^{-17}	1.08×10^{-6}	8.02×10^{-21}
$UO_2SO_{4(aq)}$	4.08×10^{-12}	1.86×10^{-10}	4.78×10^{-8}	5.95×10^{-14}
SeO_3^{2-}	6.54×10^{-21}	5.57×10^{-8}	2.71×10^{-6}	1.55×10^{-34}
HSe^-	2.29×10^{-98}	2.01×10^{-27}	6.04×10^{-23}	1.05×10^{-13}
$HSeO_3^-$	1.24×10^{-19}	2.33×10^{-4}	2.52×10^{-5}	3.86×10^{-31}
$H_2SeO_{3(aq)}$	4.59×10^{-23}	1.96×10^{-5}	4.61×10^{-9}	1.96×10^{-32}
		mineral modal abundances		
ϕ_{Pyrite}	—	0.	0.	0.02
$\phi_{Uraninite}$	—	0.	0.138	0.01
$\phi_{Selenium}$	—	0.061	0.015	0.01
ϕ	—	0.179	0.087	0.2
v/u	—	6.77×10^{-5}	8.03×10^{-5}	8.66×10^{-5}

5.3. Weathering of Alaskite

This section illustrates the application of **MPATH** to weathering of an alaskite host rock consisting of albite, K-feldspar and quartz. This example was considered previously by Helgeson and Murphy (1983) within a single reaction path framework. Rainwater modified by transport through a soil zone resulting in a pH of 4 is allowed to percolate through the host rock with the composition given in Table 2. A Darcy flow velocity of 1 m y^{-1} is assumed in the calculation. Values for kinetic rate constants and surface areas used in the calculation are given in Table 2 for primary minerals K-feldspar, albite and quartz. For kaolinite and gibbsite, values for the product of the rate constant and surface area ks of 10^{-14} moles cm^{-3} s^{-1} are used. Surface areas are calculated from Eqn.(36) using grain sizes of 1.5mm for K-feldspar and albite, and 1.125mm for quartz. The precipitation of quartz and chalcedony, which are unlikely to form under weathering environments due to kinetic constraints, are suppressed. Amorphous silica remains under-saturated during the calculation. A sequence of 5000 stationary states are calculated with equal time steps of 200 years yielding a total evolution time of 1,000,000 years.

Table 2: Initial volume fractions, kinetic rate constants, enthalpies of activation and surface areas used in the calculations describing weathering and hydrothermal alteration of alaskite.

mineral	ϕ_m^0	k_m^0	$\Delta H_m^\dagger$	s_m
	.	(moles $cm^{-2}sec^{-1}$)	(kcal $mole^{-1}$)	(cm^{-1})
K-feldspar	0.40	3.0×10^{-16}	8.5	16.0
albite	0.15	3.0×10^{-16}	8.5	8.0
quartz	0.40	1.0×10^{-16}	18.5	16.0

The volume fractions for primary and secondary minerals are shown in Fig. 11 plotted as a function of distance for elapsed times of 10,000, 50,000, 100,000 and 1,000,000 years. Two zones of kaolinite form separated by muscovite (used as a surrogate for illite). This zone sequence would be difficult if not impossible to predict merely from an equilibrium activity diagram. Albite completely dissolves at the surface of the weathering column after approximately 35,000 years and K-feldspar after about 95,000 years. For times less than this, alteration zones of gibbsite, kaolinite and muscovite form in place with little downward migration. For times greater than this, however, substantial migration of the alteration zones

take place. In addition a different reaction mechanism is responsible for their growth. For early times the alteration zones are formed directly from the dissolution of primary minerals albite and K-feldspar. However, at later times when all the primary minerals have completely dissolved at

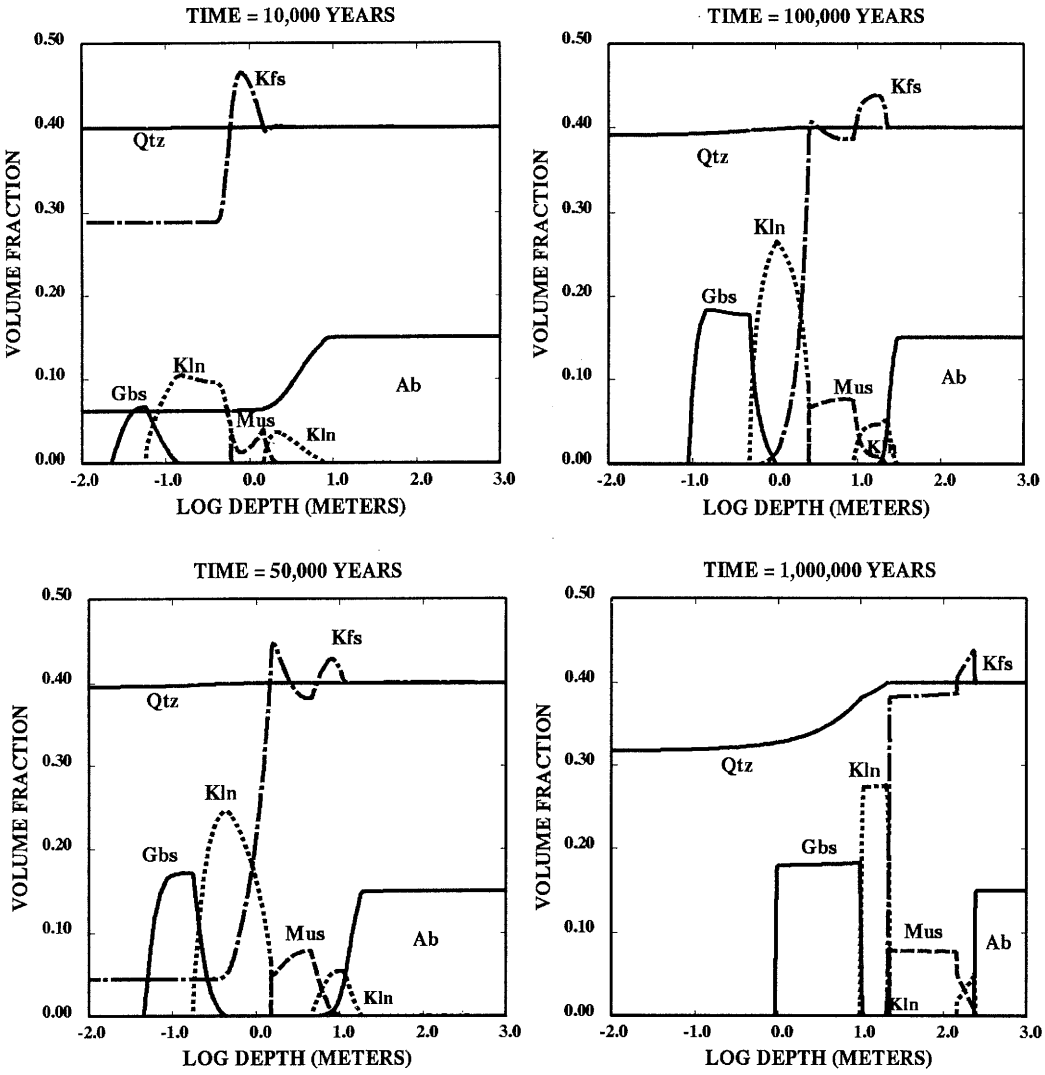

Figure 11: Weathering profiles for the alteration of alaskite assuming a Darcy velocity of 1 m y^{-1} for elapsed times of 10,000, 50,000, 100,000 and 1,000,000 years. The precipitation of quartz and chalcedony are suppressed. Kaolinite forms two distinct reaction zones located at the K-feldspar and albite dissolution fronts. Abbreviations used in the figure are: quartz (Qtz), gibbsite (Gbs), kaolinite (Kln), K-feldspar (Kfs), muscovite (Mus) and albite (Ab).

the top of the weathering column, gibbsite forms from kaolinite, and the upper kaolinite zone

forms from muscovite. The muscovite zone forms both from dissolution of kaolinite and primary K-feldspar and albite. After an elapsed time of one million years the gibbsite zone is over 10 meters thick forming a substantial ore deposit. The rate of weathering of albite is more rapid than K-feldspar in agreement with field observations. Note that authigenic K-feldspar forms within the deeper lying kaolinite and muscovite zones. The unaltered rock occurs just downstream from the top of the albite zone. The rate of weathering is rapid with a 250 meter weathered zone occurring in approximately one million years, or a rate of 2.5×10^{-4} m y^{-1}. The variation in pH with depth in the weathering column is shown in Fig. 12.

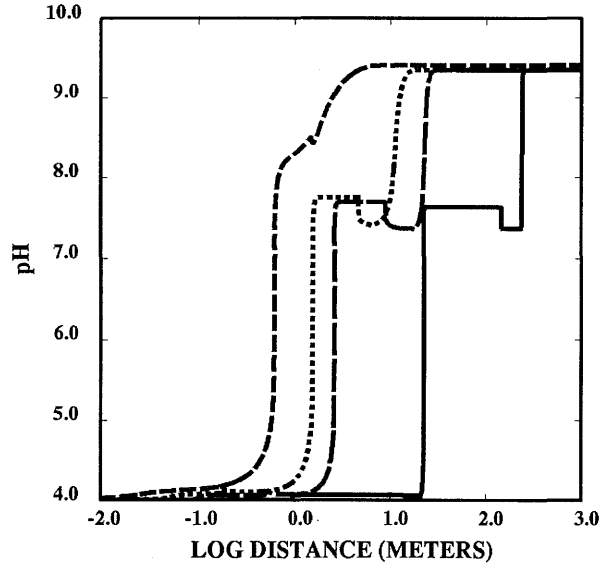

Figure 12: The variation of pH within the alaskite weathering profile plotted as a function of distance for elapsed times of 10,000 (short dashed), 50,000 (dotted), 100,000 (long dashed) and 1,000,000 (solid) years.

With increasing time reaction becomes localized at zone boundaries. Within the various zones the fluid comes to equilibrium with the minerals in the zone. As a consequence the volume fraction reaches a maximum value and continued transport and reaction results in an increase in zone width. The sharp changes in pH and mineral volume fractions indicates that the local equilibrium limit is closely achieved after this time span. Nevertheless, for this problem, there does not appear to exist a consistent solution to the transport equations for conditions of local equilibrium and pure advective transport.

5.4. Hydrothermal Alteration of Alaskite

The final example describes the hydrothermal alteration of an alaskite host rock with the same modal composition as in the previous example (see Table 2) in the presence of a temperature gradient. To illustrate the effect of heating and cooling of a fluid packet moving along the flow path, a hypothetical situation is considered in which a gaussian temperature profile is imposed on the system given by the equation

$$T(x) = T_0 + (T_{max} - T_0)\, e^{-[(x-x_0)/\alpha]^2}, \tag{93}$$

where $T_0 = 25°C$, $T_{max} = 300°C$, $\alpha = 250$ meters and $x_0 = 1000$ meters (see Fig. 13). Fluid entering the porous rock column at a temperature of 25° is heated to 300° by a constant heat source centered at a distance of 1 km from the inlet. The inlet fluid is in equilibrium with minerals albite, K-feldspar, muscovite and quartz with an assumed pH of 9. A Darcy flow velocity of 1 m y^{-1} is used in the calculation. The kinetic rate constants vary with temperature according to Eqn.(32). Values for the kinetic rate constants, surface areas and enthalpies of activation used in the calculation are given in Table 2.

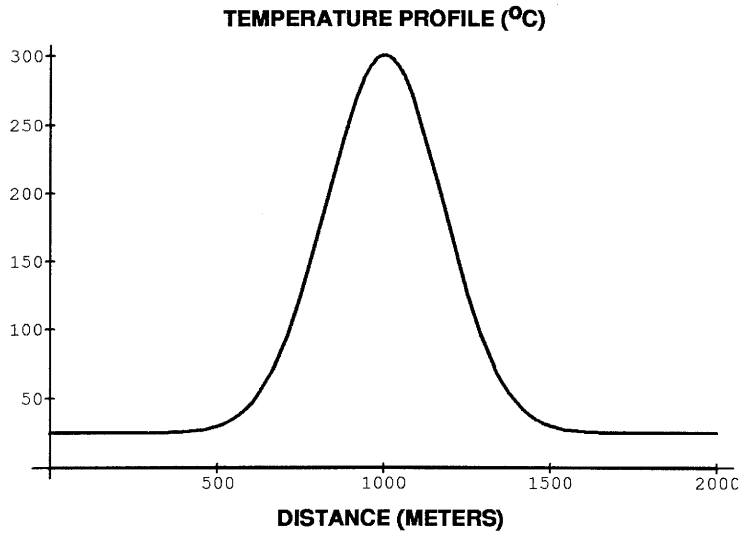

Figure 13: Gaussian temperature profile. Temperature varies from 25°C at the inlet and outlet to a maximum of 300°C in the center of the column.

The volume fractions of albite, K-feldspar and quartz are shown in Fig. 14 plotted as a function of distance for elapsed times of 25,000, 50,000, 100,000 and 200,000 years. K-

feldspar and quartz dissolve, while albite precipitates as the fluid heats up approaching the heat source. As the fluid cools on the down-gradient side of the heat source just the opposite occurs with K-feldspar and quartz precipitating and albite dissolving. Eventually a zoned rock is obtained consisting of the two zones albite + quartz and K-feldspar + quartz. With increasing time the system closes down with all available porosity taken up by precipitation of quartz on the down-gradient side of the heat source. With increasing time all available pore space is taken up by precipitation of quartz on the down-gradient side of the heat source. The reaction rates are shown in Fig. 15 corresponding to an elapsed time of 200,000 years. As is apparent from the figure both aluminum and silica are, to a good approximation, conserved during the replacement of K-feldspar by albite. Silica released by dissolution of quartz on the up-gradient side of the heat source is reprecipitated as quartz on the down-gradient side. The concentrations of solute species and the pH are shown in Fig. 16 plotted as a function of distance for the same time as in Fig. 15. The pH drops from the inlet value of 9 to approximately 7 at the peak in the heat source and then increases to 9.4 at the outlet. The pH profile is essentially independent of time, as are the other species with the exception of K^+. From this figure it is apparent from the concentration profile for $Al(OH)_4^-$ that aluminum is not strictly conserved, however its concentration is extremely small so as not to make a large difference in the overall aluminum mass balance.

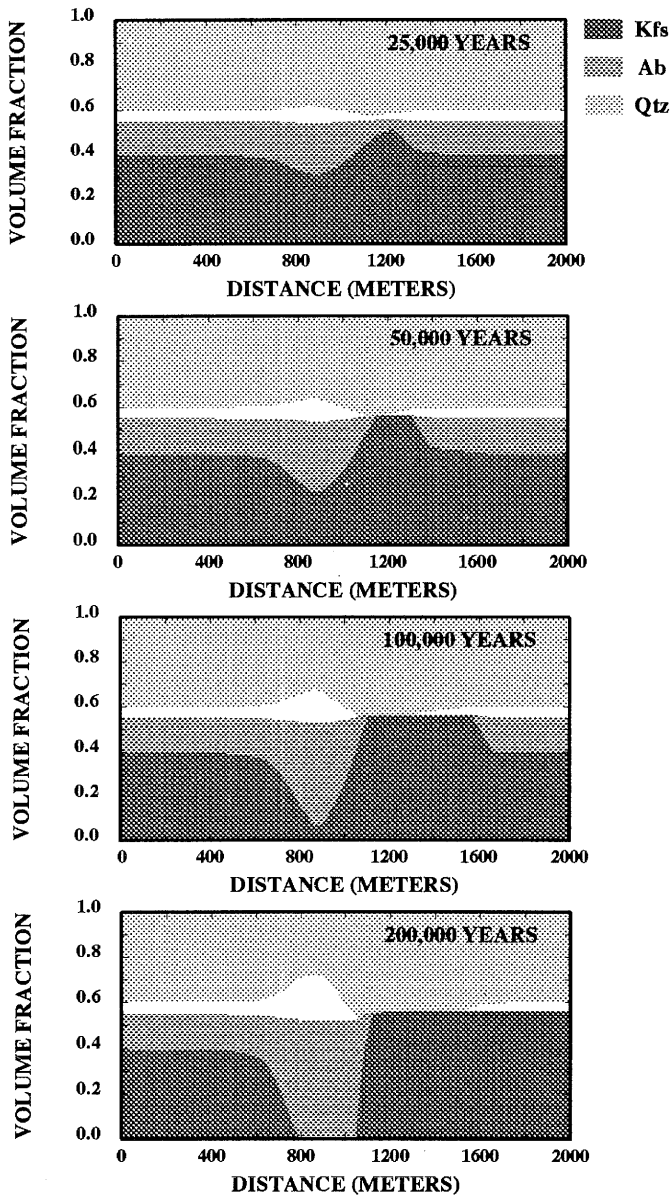

Figure 14: The volume fractions of albite, K-feldspar and quartz plotted as a function of distance for the indicated times resulting from the hydrothermal alteration of alaskite with the composition given in Table 2. On the up-gradient side K-feldspar is replaced by albite as quartz dissolves, and on the down-gradient side albite is replaced by K-feldspar as quartz precipitates. The white area designates porosity which becomes entirely filled with quartz on the down-gradient side of the heat source.

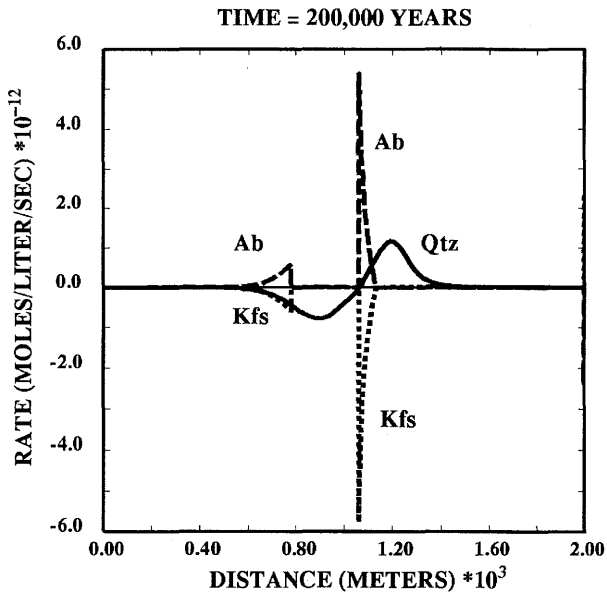

Figure 15: Mineral reaction rates plotted as a function of distance for an elapsed time of 200,000 years. Note that the reaction rates for albite and K-feldspar are equal in magnitude but opposite in sign indicating that aluminum and silica are approximately conserved by the replacement of K-feldspar by albite.

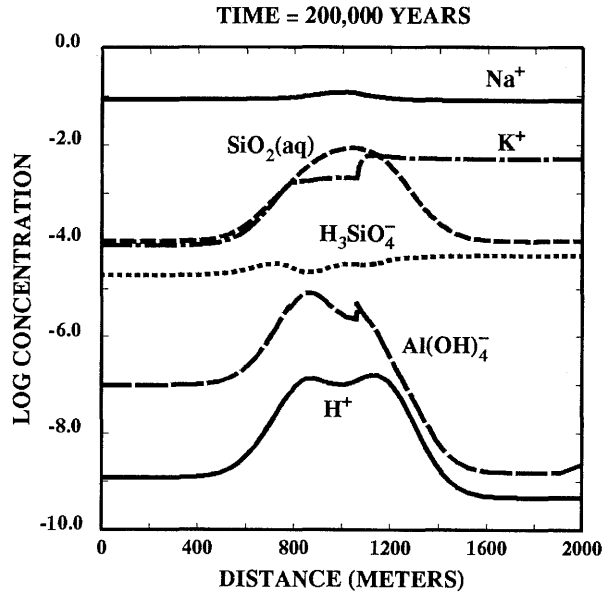

Figure 16: Solute concentrations plotted as a function of distance for an elapsed time of 200,000 years. The jumps in concentration of K^+ and $Al(OH)_4^-$ occur at the K-feldspar and albite replacement fronts, respectively.

6. DISCUSSION

The various examples considered above all illustrate the importance of integrating the mass transport equations over sufficiently long time spans. Failure to do so may lead to an incomplete picture of the time evolution of the system being studied. In general, the time evolution of any particular system described by kinetic rate laws can be divided into three overlapping stages. The first stage corresponds to early times in which alteration of the host rock takes place by direct transformation of primary minerals into secondary minerals with little movement of the reaction zones in the direction of fluid transport. During this stage primary minerals are present throughout the entire host rock. With continued fluid transport, eventually the primary minerals completely dissolve at the beginning of the alteration column, leading to the second stage of alteration. During this stage, alteration zones begin to migrate with time. In the region where primary minerals are absent, secondary minerals are formed by dissolving other secondary minerals deposited previously during the first stage of alteration. At the interface between the unaltered host rock and altered rock, secondary minerals are created as primary minerals dissolve. As mineral alteration zones grow with time, reaction tends to become more and more localized at zone boundaries. This is a consequence of the reaction zones becoming sufficiently wide so that a fluid packet is able to reach equilibrium with the minerals in the interior of the zone. The final stage is marked by the formation of a steady-state in which mineral alteration zones propagate with constant velocities. (This steady-state limiting form of the solution is not to be confused with the stationary states used to construct the time evolution of the system.) Mineral abundances reach their maximum values as a steady-state is approached. The kinetic based, steady-state solution exhibits certain similarities with the corresponding local equilibrium solution, provided it exists. Solute concentrations and mineral abundances are the same in the two descriptions, except in the immediate vicinity of reaction fronts, and reaction front velocities are equal. Only the widths of reaction zones differ between the two descriptions. This is caused, primarily, by the non-existence of the first stage of alteration in a local equilibrium description. In the case of local equilibrium, mineral alteration zones are formed immediately as the inlet fluid commences to react with the host rock completely dissolving the primary minerals at the inlet. Thus in this case there does not exist a period of evolution in which primary minerals remain present over the entire flow path as secondary minerals are formed. Rather alteration zones propagate instantaneously beginning with infinitesimal widths with reactions

taking place at sharp reaction fronts. By contrast, in a kinetic description considerable time may pass, depending on the system, during which primary minerals are slowly altered to secondary minerals, thereby creating secondary alteration zones with a finite initial width.

There are several reasons why this simple picture of a one-dimensional system undergoing chemical alteration may not hold. A number of complicating factors have not been considered in the evolution of the system. These include changes in porosity and permeability which may make it impossible for a steady-state to be achieved. In addition, two-dimensional aspects of the flow system may result in a fingering behavior of reaction fronts also leading to a non-steady state behavior. Double porosity effects with transport taking place simultaneously in fractures and the rock matrix can be expected to qualitatively alter the behavior of the system as well.

7. CONCLUSION

The main purpose of this contribution is to develop a numerical algorithm applicable to integrating mass transport equations representing fluid-rock interaction over geologic time spans. Emphasis is placed on the influence of long time spans of hundreds of thousands to millions of years or more on the evolution of natural geochemical processes involving fluid-rock interaction. This is an essential aspect of a quantitative description of solute transport and chemical reactions involving not only natural process, but also for analyzing the disposal of long-lived radionuclides by underground burial. The ability to carry out the integration of multicomponent mass transport equations over long time spans requires the introduction of simplifications based on the quasi-stationary state approximation, or multiple reaction path formulation, of the transport-reaction problem. By contrast, for very short time scales on the order of years to at most a few hundred years typical of many engineering problems, conventional finite-difference or finite-element algorithms are adequate for solving the transient mass transport equations. The quasi-stationary state approximation enables integration of the governing mass transport equations over geologic time spans while taking into account the full complexity of chemical reactions in as sophisticated a manner as found in conventional distribution of species computer programs such as **EQ3** (Wolery, 1987). In addition, it is possible to monitor the accuracy of the solution by verifying global mass conservation conditions and, in certain cases, by comparing the solution obtained for long time spans with the corresponding solution obtained

directly from non-linear algebraic equations representing conditions of local equilibrium and pure advective transport. It should be emphasized that the quasi-stationary state approximation applies also to transport involving diffusion and dispersion, and is not restricted to pure advective transport.

The multiple reaction path approach was implemented in the computer code **MPATH** which enables prediction of the time evolution of complex natural systems involving pure advective fluid transport and chemical reactions over geologic time spans. Several examples were given of the application of **MPATH** to redox problems, weathering and hydrothermal alteration. A characteristic feature of all of these examples is the qualitative change in the behavior of the system with increasing time. For this reason it is essential to carry out the calculations for sufficiently long time spans.

The code **MPATH** may be extended in several different ways taking into account the computational advantages of the quasi-stationary state approximation. These include: (1) incorporating ion-exchange reactions, (2) adding diffusive and dispersive transport, (3) allowing for changes in porosity, permeability and fluid flow rate with time and distance, and (4) extension to more than a single spatial dimension. An important area of research is applying the mass transport equations to hierarchial porous media, such as a double porosity model, providing for simultaneous transport in a fracture network and rock matrix. However the computational effort for such a description would be enormous and probably must await the availability of massively parallel computer architectures before such calculations become feasible.

8. ACKNOWLEDGEMENTS

This report benefited greatly from reviews by Ian McKinley, Carl Steefel, Bill Murphy, W. Pfingsten, and Randy Arthur.

9. REFERENCES

Aagaard, P. and Helgeson, H. C. (1982) Thermodynamic and kinetic constraints on reaction rates among minerals and aqueous solutions. I. Theoretical considerations. *Am. J. Sci.* **282,** 237–285.

Biino, G. G. and Lichtner, P. C. (1992) A first principles approach to supergene enrichment of a porphyry copper protore. II. Interaction with gangue minerals. In preparation.

Haar, L., Gallagher, J. S., and Kell, G. S., Thermodynamic properties for fluid water, in Straub, J., and Scheffler, K. eds., *Water and Steam: Their Properties and Current Industrial Applications:* New York, Pergamon, 69–82, 1980.

Helgeson, H. C. (1968) Evaluation of irreversible reactions in geochemical processes involving minerals and aqueous solutions I. Thermodynamic relations. *Geochim. Cosmochim. Acta* **32,** 853–877.

Helgeson, H. C. and Murphy, W. M. (1983) Calculation of mass transfer as a function of time and surface area in geochemical processes I. Computational approach, *Math. Geol.* **15,** 109–130.

Helgeson, H. C., Murphy, W. M. and Aagaard P. (1984) Thermodynamic and kinetic constraints on reaction rates among minerals and aqueous solutions. II. Rate constants, effective surface area, and the hydrolysis of feldspar, *Geochimica et Cosmochimica Acta*, **48,** 2405–2432.

Johnson, J. W., Oelkers, E. H. and Helgeson, H. C. (1991) *SUPCRT92:* A software package for calculating the standard molal thermodynamic properties of minerals, gases, aqueous species, and reactions from 1 to 5000 bars and 0°C to 1000°C, *Computers in Geosciences*, in press.

Lichtner P. C. (1985) Continuum model for simultaneous chemical reactions and mass transport in hydrothermal systems, *Geochimica et Cosmochimica Acta*, **49,** 779–800.

Lichtner, P. C. (1986) Multiple reaction path model describing mass transfer in geochemical systems. In *Proceedings of the workshop on Geochemical Modeling*. Eds. Jackson, K. J. and Bourcier W. L. Fallen Leaf Lake, CA, September 14-17, 3–9.

Lichtner, P. C. (1988) The quasi-stationary state approximation to coupled mass transport and fluid-rock interaction in a porous medium, *Geochimica et Cosmochimica Acta* **52,** 143–165.

Lichtner, P. C. (1991) The quasi-stationary state approximation to fluid-rock interaction: local equilibrium revisited, ed. Ganguly, *Advances in Physical Geochemistry* **8,** 452–560.

Lichtner P. C. (1992) Scaling properties of kinetic mass transport equations and the local equilibrium limit, *Am. J. Sci.,* submitted for publication.

Lichtner, P. C. and Balashov, V. N. (1992) Metasomatic zoning: appearance of ghost zones in limit of pure advective mass transport, *Geochim. Cosmochim. Acta*, submitted for publication.

Lichtner, P. C. and Biino, G. G. (1992) A first principles approach to supergene enrichment of a porphyry copper protore. I. Cu–Fe–S–H_2O subsystem, *Geochim. Cosmochim. Acta*, in press.

Lichtner, P. C. and Waber, N. (1992) Redox front geochemistry and weathering: Theory with application to the Osamu Utsumi uranium mine, Poços de Caldas, Brazil, *Journal of Geochemical Exploration,* in press.

Lichtner, P. C., Helgeson, H. C., and Murphy, W. M. (1987) Lagrangian and Eulerian representations of metasomatic alteration of minerals. In *Proc. NATO Advanced Study Institute on Chemical Transport in Metasomatic Processes*, edited by H. C. Helgeson, pp. 519–545, Reidel, Dordrecht, Holland.

Murphy, W. M., Oelkers, E. H., and Lichtner, P. C. (1989) Surface reaction versus diffusion control of mineral dissolution and growth rates in geochemical processes: *Chemical Geology,* **78,** 357–380.

Nagy, K. L., Blum, A. E. and Lasaga, A. C. (1991) Dissolution and precipitation kinetics of kaolinite at 80°C and pH 3: the dependence on solution saturation state, *Am. J. Sci.* **291**, 649–686.

Ortoleva, P., Merino, E., Moore, C. H., and Chadam, J. (1987) Geochemical self–organization, I: reaction–transport feedbacks and modeling approach, *Am. J. Sci.* **287**, 979–1007.

Press, W. H., Flannery, B. P., Teukolsky, S. A. and Vetterliung, T. W. (1987) *Numerical Recipes, The Art of Scientific Computing*, Cambridge University Press, 818 pp.

Schechter, R. S., Bryant, S. L., and Lake, L. W. (1987) Isotherm–free chromatography: propagation of precipitation/dissolution waves, *Chem. Eng. Comm.* **58**, 353–376.

Steefel, C. I. and Van Cappellen, P., 1990, A new kinetic approach to modeling water–rock interaction. The role of nucleation, precursors, and Ostwald ripening: *Geochim. Cosmochim. Acta,* v. 54, 2657–2677.

Walsh, M. P., Bryant, S. L., Schechter, R. S., and Lake, L. W. (1984) Precipitation and dissolution of solids attending flow through porous media, *Amer. Inst. Chem. Eng. J.* **30**, 317–327.

Wolery, T. J. (1987) The computer code for reaction–path modeling of aqueous geochemical systems: user's guide and documentation. Lawrence Livermore National Laboratory, Livermore, CA, UCRL report in preparation.

APPENDIX A: EXPLICIT EXAMPLE OF TRANSPORT EQUATIONS

In this appendix the transport equations are written out in full for the problem of weathering of K-feldspar (Kfs). In this problem three possible secondary minerals are considered: gibbsite (Gbs), kaolinite (Kln) and illite (Mus) (represented by muscovite). In addition there are several dominant aqueous complexes that must be taken into account. These are complexes with aluminum: $Al(OH)_4^-$, $Al(OH)_3$, $Al(OH)_2^+$ and $AlOH^{2+}$; with aqueous silica: $H_3SiO_4^-$; and the OH^- complex. These minerals and aqueous species may be expressed in terms of the primary species Al^{3+}, H^+, SiO_2 and K^+ according to the reactions:

$$K^+ + Al^{3+} + SiO_2 - 4H^+ + 2H_2O \rightleftharpoons Kfs, \tag{A.1}$$

$$K^+ + 3Al^{3+} + 3SiO_2 - 10H^+ + 6H_2O \rightleftharpoons Mus, \tag{A.2}$$

$$2Al^{3+} + 2SiO_2 - 6H^+ + 5H_2O \rightleftharpoons Kln, \tag{A.3}$$

$$Al^{3+} + 3H_2O - 3H^+ \rightleftharpoons Gbs, \tag{A.4}$$

for minerals, and

$$Al^{3+} + 4H_2O - 4H^+ \rightleftharpoons Al(OH)_4^-, \tag{A.5}$$

$$Al^{3+} + 3H_2O - 3H^+ \rightleftharpoons Al(OH)_3, \tag{A.6}$$

$$Al^{3+} + 2H_2O - 2H^+ \rightleftharpoons Al(OH)_2^+, \tag{A.7}$$

$$Al^{3+} + H_2O - H^+ \rightleftharpoons AlOH^{2+}, \tag{A.8}$$

$$SiO_2 - H^+ + 2H_2O \rightleftharpoons H_3SiO_4^-, \tag{A.9}$$

$$H_2O - H^+ \rightleftharpoons OH^-, \tag{A.10}$$

for aqueous complexes. The corresponding generalized concentrations Ψ_j for $j = K^+, Al^{3+}, H^+, SiO_2$ corresponding to the above set of primary species are defined by

$$\Psi_{K^+} = C_{K^+}, \tag{A.11}$$

$$\Psi_{Al^{3+}} = C_{Al^{3+}} + C_{Al(OH)_4^-} + C_{Al(OH)_3} + C_{Al(OH)_2^+} + C_{AlOH^{2+}}, \tag{A.12}$$

$$\Psi_{H^+} = C_{H^+} - C_{OH^-} - 4C_{Al(OH)_4^-} - 3C_{Al(OH)_3} - 2C_{Al(OH)_2^+} - C_{AlOH^{2+}} - C_{H_3SiO_4^-}, \tag{A.13}$$

$$\Psi_{SiO_2} = C_{SiO_2} + C_{H_3SiO_4^-}. \tag{A.14}$$

Note that the quantities Ψ_{K^+}, $\Psi_{Al^{3+}}$ and Ψ_{SiO_2} correspond to the total concentration of the corresponding primary species, whereas Ψ_{H^+} does not represent the total amount of hydrogen ions in solution and may in fact become negative depending on the pH. Water is considered to be in sufficiently large abundance that its activity may be taken equal to unity and therefore this species does not appear in the transport equations. The mass transport equations for aqueous species expressed in terms of the generalized concentrations are given by

$$\widehat{\mathcal{L}}[K^+] = -I_{Kfs} - I_{Mus}, \tag{A.15}$$

$$\widehat{\mathcal{L}}[Al^{3+}] = -I_{Kfs} - 3I_{Mus} - 2I_{Kln} - I_{Gbs}, \tag{A.16}$$

$$\widehat{\mathcal{L}}[H^+] = 4I_{Kfs} + 10I_{Mus} + 6I_{Kln} + 3I_{Gbs}, \tag{A.17}$$

$$\widehat{\mathcal{L}}[SiO_2] = -I_{Kfs} - 3I_{Mus} - 2I_{Kln}, \tag{A.18}$$

with the differential operator $\widehat{\mathcal{L}}$ defined by

$$\widehat{\mathcal{L}} = \left[\frac{\partial}{\partial t}\phi - \frac{\partial}{\partial x}\phi D \frac{\partial}{\partial x} + u\frac{\partial}{\partial x}\right]\Psi. \tag{A.19}$$

The mineral mass transfer equations are given by

$$\frac{\partial \phi_{Kfs}}{\partial t} = \bar{V}_{Kfs} I_{Kfs}, \tag{A.20}$$

$$\frac{\partial \phi_{Gbs}}{\partial t} = \bar{V}_{Gbs} I_{Gbs}, \tag{A.21}$$

$$\frac{\partial \phi_{Kln}}{\partial t} = \bar{V}_{Kln} I_{Kln}, \tag{A.22}$$

$$\frac{\partial \phi_{Mus}}{\partial t} = \bar{V}_{Mus} I_{Mus}. \tag{A.23}$$

In the case of the quasi-stationary state approximation the partial time derivatives in the transport equations for solute species are neglected and the equations become ordinary differential equations in the space coordinate alone.

APPENDIX B: TRANSFORMATION OF PRIMARY SPECIES

It is advantageous to transform the primary species to a new set with dominant concentrations to improve the efficiency of numerical computations. Such a transformation is especially important when a reaction path traverses a redox front. Usually the species $O_{2(aq)}$ is used to represent the redox state on the oxidized side of the front. But on the reduced side of the front where the concentration of $O_{2(aq)}$ is essentially zero some other redox pair must be used. Such a transformation is essential for describing secondary mineralization. Similar problems occur for the aluminum species as the pH of the system changes from low values where the species Al^{3+} is the dominate species, to higher values where the complex $Al(OH)_4^-$ is dominant.

For a given set of primary species denoted by $\{\mathcal{A}_j\}$, the chemical reactions taking place in the system can be expressed according to Eqns.(1), (2) and (3). For some other choice of primary species denoted by $\{\mathcal{A}'_j\}$, the reactions have the identical form as above with ν_{ji}^{rev} and ν_{ji}^{kin} replaced by $\nu_{ji}^{rev'}$ and $\nu_{ji}^{kin'}$ respectively, and ν_{jm} replaced by ν'_{jm}:

$$\sum_{j=1}^{N} \nu_{ji}^{rev'} \mathcal{A}'_j \rightleftharpoons \mathcal{A}'_i, \tag{B.1}$$

$$\sum_{j=1}^{N} \nu_{ji}^{kin'} \mathcal{A}'_j \rightleftharpoons \mathcal{A}'_i, \tag{B.2}$$

and

$$\sum_{j=1}^{N} \nu'_{jm} \mathcal{A}'_j \rightleftharpoons \mathcal{M}_m, \tag{B.3}$$

where A'_i denotes the transformed secondary species. The transport equations for the transformed primary species have the identical form as the original equations

$$\frac{\partial}{\partial t}(\phi \Psi'_j) + \nabla \cdot \Omega'_j = -\sum_m \nu'_{jm} I'_m, \tag{B.4}$$

where the generalized concentration and flux are given respectively by

$$\Psi'_j = C'_j + \sum_i \nu_{ji}^{rev'} C'_i + \sum_l \nu_{jl}^{kin'} C'_l, \tag{B.5}$$

and

$$\Omega'_j = J'_j + \sum_i \nu_{ji}^{rev'} J'_i + \sum_l \nu_{jl}^{kin'} J'_l. \tag{B.6}$$

To obtain an explicit expression for the transformed stoichiometric matrices $\nu^{rev\prime}_{ji}$, $\nu^{kin\prime}_{ji}$ and ν'_{jm}, corresponding equilibrium constants, and the generalized concentration Ψ'_j and flux Ω'_j in terms of the original quantities, it is sufficient to consider the interchange of a single primary species with a reversible aqueous secondary species. A general transformation can then be made up of a sequence of such elementary transformations. For the interchange of the j_0th primary species with the i_0th secondary species, the transformed species are related according to

$$\mathcal{A}'_{j_0} = \mathcal{A}_{i_0}, \tag{B.7}$$

$$\mathcal{A}'_{i_0} = \mathcal{A}_{j_0}, \tag{B.8}$$

$$\mathcal{A}'_j = \mathcal{A}_j \quad (j \neq j_0), \tag{B.9}$$

$$\mathcal{A}'_i = \mathcal{A}_i \quad (i \neq i_0). \tag{B.10}$$

The concentrations of aqueous species are transformed according to the relations

$$C'_{j_0} = C_{i_0}, \tag{B.11}$$

$$C'_{i_0} = C_{j_0}, \tag{B.12}$$

$$C'_j = C_j, \quad (j \neq j_0), \tag{B.13}$$

$$C'_i = C_i, \quad (i \neq i_0). \tag{B.14}$$

The concentration of the j_0th primary species can be expressed in terms of the concentration of the i_0th secondary species by solving the mass action equation for m_{i_0} in terms of m_{j_0} resulting in the relation:

$$m_{j_0} = \gamma_{j_0}^{-1} K_{i_0}^{-1/\nu_0} (\gamma_{i_0} m_{i_0})^{1/\nu_0} \prod_{j \neq j_0} (\gamma_j m_j)^{-\nu_{ji_0}/\nu_0}, \tag{B.15}$$

where ν_0 is defined by

$$\nu_0 = \nu^{rev}_{j_0 i_0}. \tag{B.16}$$

Substituting this result into the mass action equation for the ith reversible aqueous complex with $i \neq i_0$, yields

$$m_i = \gamma_i^{-1} K_i K_{i_0}^{-\nu_{j_0 i}/\nu_0} (\gamma_{i_0} m_{i_0})^{\nu_{j_0 i}/\nu_0} \prod_{j \neq j_0} (\gamma_j m_j)^{[\nu_{ji} - \nu_{ji_0}\nu_{j_0 i}/\nu_0]}. \tag{B.17}$$

This relation must be of the form

$$m_i = m'_i = \gamma_i'^{-1} K'_i \prod \left(\gamma'_j m'_j\right)^{\nu^{rev\prime}_{ji}}. \tag{B.18}$$

Comparing powers of m_j yields an expression for the transformed stoichiometric matrix $\nu_{ji}^{rev\prime}$ for reversible aqueous complexes in terms of the original stoichiometric matrix ν_{ji}^{rev} according to the relations

$$\nu_{ji}^{rev\prime} = \nu_{ji}^{rev} - \frac{\nu_{ji_0}^{rev}\nu_{j_0i}^{rev}}{\nu_0} \quad (j \neq j_0,\ i \neq i_0), \tag{B.19}$$

$$\nu_{ji_0}^{rev\prime} = -\frac{\nu_{ji_0}^{rev}}{\nu_0} \quad (j \neq j_0), \tag{B.20}$$

$$\nu_{j_0i}^{rev\prime} = \frac{\nu_{j_0i}^{rev}}{\nu_0} \quad (i \neq i_0), \tag{B.21}$$

and

$$\nu_0{}' = \frac{1}{\nu_0} \quad (j = j_0). \tag{B.22}$$

The corresponding equilibrium constants transform according to the expressions

$$\log K'_i = \log K_i - \frac{\nu_{j_0i}^{rev}}{\nu_0}\log K_{i_0}, \tag{B.23}$$

and

$$\log K'_{i_0} = -\log K_{i_0}/\nu_0. \tag{B.24}$$

The stoichiometric reaction matrix for mineral reactions transforms according to

$$\nu'_{jm} = \nu_{jm} - \frac{\nu_{ji_0}^{rev}\nu_{j_0m}}{\nu_0} \quad (j \neq j_0), \tag{B.25}$$

and

$$\nu'_{j_0m} = \frac{\nu_{j_0m}}{\nu_0} \quad (j = j_0). \tag{B.26}$$

The corresponding equilibrium constant transforms according to

$$\log K'_m = \log K_m - \frac{\nu_{j_0m}}{\nu_0}\log K_{i_0}. \tag{B.27}$$

Likewise an expression for the transformed stoichiometric matrix $\nu_{ji}^{kin\prime}$ for irreversible aqueous complexes is given by the relations

$$\nu'^{kin}_{jl} = \nu_{jl}^{kin} - \frac{\nu_{ji_0}^{rev}\nu_{j_0k}^{kin}}{\nu_0} \quad (j \neq j_0), \tag{B.28}$$

and

$$\nu'^{kin}_{j_0k} = \frac{\nu_{j_0k}^{kin}}{\nu_0} \quad (j = j_0). \tag{B.29}$$

The corresponding equilibrium constant transforms according to

$$\log K'_l = \log K_l - \frac{\nu_{j_0l}}{\nu_0}\log K_{i_0}. \tag{B.30}$$

The generalized concentration and flux transform according to

$$\Psi'_j = \Psi_j - \frac{\nu^{rev}_{ji_0}}{\nu_0}\Psi_{j_0} \quad (j \neq j_0), \tag{B.31}$$

$$= \frac{1}{\nu_0}\Psi_{j_0} \quad (j = j_0), \tag{B.32}$$

and

$$\Omega'_j = \Omega_j - \frac{\nu^{rev}_{ji_0}}{\nu_0}\Omega_{j_0} \quad (j \neq j_0), \tag{B.33}$$

$$= \frac{1}{\nu_0}\Omega_{j_0} \quad (j = j_0). \tag{B.34}$$

APPENDIX C: JACOBIAN MATRIX

The Jacobian matrix corresponding to the finite-difference equations given by Eqns.(67) and (68) for the residual functions has the form

$$\frac{\partial R_j}{\partial C_{j'}} = \frac{\partial \Psi_j}{\partial C_{j'}} + \lambda \frac{\Delta x}{u} \sum_{m=1}^{M} \nu_{jm} \frac{\partial I_m}{\partial C_{j'}}, \tag{C.1}$$

$$\frac{\partial R_j}{\partial C_{l'}} = 0, \tag{C.2}$$

$$\frac{\partial R_l}{\partial C_{j'}} = -\lambda \frac{\Delta x}{u} \frac{\partial I_l^{kin}}{\partial C_{j'}}, \tag{C.3}$$

$$\frac{\partial R_l}{\partial C_{l'}} = \delta_{ll'} - \lambda \frac{\Delta x}{u} \frac{\partial I_l^{kin}}{\partial C_{l'}}. \tag{C.4}$$

The derivatives of the generalized concentration Ψ_j are given by

$$\frac{\partial \Psi_j}{\partial C_{j'}} = \delta_{jj'} + \sum_i \nu_{ji} C_i \left(\frac{1}{C_{j'}} \nu_{j'i} + \frac{\partial I}{\partial m_j} \left[\sum_k \nu_{ki} \frac{d \ln \gamma_k}{dI} - \frac{d \ln \gamma_i}{dI} \right] \right). \tag{C.5}$$

The derivatives of the reaction rates I_m and I_l^{kin} appearing in these equations are given by

$$\frac{\partial I_m}{\partial m_j} = k_m K_m Q_m \left(\frac{1}{m_j} \nu_{jm} + \frac{\partial I}{\partial m_j} \sum_k \nu_{km} \frac{d \ln \gamma_k}{dI} \right). \tag{C.6}$$

$$\begin{aligned} \frac{\partial I_l^{kin}}{\partial m_j} = {} & k_l^f Q_l^f \left(\frac{1}{m_j} \nu_{jl}^{kin} \delta(\nu_{jl}) + \frac{\partial I}{\partial m_j} \sum_{l', \nu_{l'k}^{kin} > 0} \nu_{lk}^{kin} \frac{d \ln \gamma_{l'}}{dI} \right) \\ & - k_l^b Q_l^b \left(\frac{1}{m_j} (-\nu_{jl}^{kin}) \delta(-\nu_{ji}) + \frac{\partial I}{\partial m_j} \sum_{l', \nu_{l'k}^{kin} < 0} (-\nu_{lk}^{kin}) \frac{d \ln \gamma_l}{dI} \right), \end{aligned} \tag{C.7}$$

and

$$\frac{\partial I_l^{kin}}{\partial m_{l'}} = -k_l^b Q_l^b \left(\frac{1}{m_l} \delta_{ll'} + \frac{d \ln \gamma_l}{dI} \frac{\partial I}{\partial C_{l'}} \right). \tag{C.8}$$

Partial derivatives of the ionic strength I with respect to the concentrations of the primary species can be expressed in the form

$$\frac{\partial I}{\partial m_j} = \frac{z_j^2/2 + \sum_i \nu_{ji} z_i^2 m_i^{rev}/(2 m_j)}{1 - \frac{1}{2} \sum_i z_i^2 m_i^{rev} \left[\sum_k \nu_{ki} d \ln \gamma_k / dI - d \ln \gamma_i^{rev} / dI \right]}, \tag{C.9}$$

and for the lth irreversible aqueous complex

$$\frac{\partial I}{\partial m_l} = \frac{1}{2} z_l^2. \tag{C.10}$$

Derivatives of the activity coefficients with respect to the ionic strength follow directly from the definition of γ_l and the ionic strength according to

$$\frac{d \log \gamma_l}{dI} = -\frac{1}{2} \frac{A z_l^2}{I^{1/2} (1 + B \text{å}_l I^{1/2})^2} + \dot{b}. \tag{C.11}$$